RAM ROBOTICS AND MECHATRONICS

Experimental Evaluation of a Safety Aware Impedance Controller Design

F. (Frank) Weijers

MSc Report

Committee:
Prof.dr.ir. S. Stramigioli
Dr.ir. T.J.A. de Vries
Dr. T.S. Tadele
Dr.ir. A.H.A. Stienen
D. Dresscher, MSc

May 2015

011RAM2015
Robotics and Mechatronics
EE-Math-CS
University of Twente
P.O. Box 217
7500 AE Enschede
The Netherlands

UNIVERSITY OF TWENTE.

MIRA BIOMEDICAL TECHNOLOGY AND TECHNICAL MEDICINE

CTIT

Abstract

During this master project the proposed safety aware impedance controller of Tadele et al. (2014b) has been evaluated experimentally. This controller is designed to be used on the Phillips Robotic Arm (PRA) used during the BOBBIE project. Within in this project a controller is requested which is able to safely interact with its environment. To test the proposed controller, the robotic arm of the KUKA youBOT is used. This manipulator is also able to perform different tasks in multiple degrees of freedom, like the PRA, however, it is better suited as a test platform.

Two different joints of the KUKA youBOT are used during the experiment to first obtain measurements in joint space by using the one degree of freedom implementation. After these measurement the controller is evaluated using the proposed controller in cartesian space. During the experiment it was noticed that the controller was suffering from the available friction in the joints, therefore a plant compensation controller is designed to compensate for this friction.

The performed experiments have shown that the controller remains stable while the control parameters are changed to maintain the desired power and energy limits. By adding the plant compensation controller the friction was compensated however, this interferes with the passivity of the controlled system. Therefore it will be advised to partially compensate for friction such that no overcompensation occurs.

Contents

1 Introduction

Nowadays, there is an introduction of domestic robots in the health care to help people who are not able to take care of themselves and to reduce the work load of the nurses. These robots have to interact safely with their environment, which is in most cases unknown. Therefore, the control algorithm of the robot needs to have a protection layer which prevents it from causing dangerous situations with the people around it. In the study of Ikuta et al. (2003) a proposal to measure certain risks is given. These risks are divided in three different classes:

- mechanical injury
- electrical injury
- acoustic injury

Of the above shown classes only the mechanical injuries can be limited with proper control strategies, therefore the given paper considers only this type of injury. To address safety concerns and analyse injury risks, researchers propose a danger-index what can be used to calculate the risk of an injury. The formula uses critical parameters which can be obtained for different body parts of the human. By minimizing this danger index, certain types of injuries can be prevented when a robot interacts with a person. In the research of Haddadin et al. (2008) it is investigated what kind of injuries can be caused by human-robot interaction and how to prevent them. During this research they focus on head injuries. These injuries are caused in two different cases: when the head is clamped against a wall and when the head can move freely. They use the Head Injury Criterion (HIC), which is used in the automobile industry, to measure the impact of a certain force on the head. By using different masses and velocities of the robotics arm, the researchers concluded what kinds of injuries are caused during impact. To limit the impact force and velocity of a robotic arm, a controller has to be designed which is able to limit these parameters. Another controller design approach that addresses safety issues of robotic manipulators used in human present environments was proposed by (Tadele et al., 2014b). In this research, an impedance controller is proposed to be applied on a manipulator which is used in a domestic environment. This controller uses the standard design of an impedance controller and is extended with power and energy based safety norms. To maintain energy consistency, and passivity an energy tank based system is used. The used norms are derived using the maximum energy that a human can withstand without having serious injuries.

The controller is designed to be used within the BOBBIE project (Bobbie Robotics, 2014) where a robot has been developed for operating in a domestic environment. The robot used in the project uses a 7 degree of freedom (DOF) robotic arm, the Philips Robotic Arm (PRA). This robotic arm is designed such that it mimics the kinematics of the human arm (de Boer, 2012). As the PRA is mechanical complicated, it is chosen to use the KUKA youBot(KUKA Laboratories, 2014) as a test platform. This robot has a 5 DOF robotic arm and is commonly used as control platform. The safety aware controller design proposed for robotic manipulators was experimentally evaluated in a simple 1-DOF manipulator and was not validated in a practical multi-DOF setting. This Master project addresses the implementation of the controller in a multi-DOF manipulator by using the KUKA youBot as a test plat form. Various scenarios will be given to test the capabilities of the controller on a multi-dimensional manipulator. Furthermore a feed forward controller will be designed to compensate for friction which is present in the joints. At the end of the project, the KUKA robot arm should be able to safely interact which its environment, causing no injuries or damage.

2 Background

Within this chapter the background information will be given which will be used during this project. First the KUKA youBot, which will be used as a test platform, will be discussed. This will contain a short introduction of the KUKA youBot by giving the dynamical model of this manipulator. In the following section the impedance controller will be explained which is used as the base of the proposed controller. As last part of this chapter, the proposed extensions will be explained.

2.1 General Outline KUKA youBot

Before the controller will be implemented on the real system, it will be first tested with a model of the manipulator. In a simulation program the control parameters can be obtained and verified before the controller is implemented in the real system. A kinematic model of the KUKA youBot has already been made within the master thesis of D.Dresscher (2011). In this section only the arm of the youBot will be discussed because this part will be used only during this master assignment. The robotic arm of the youBot consist of 6 links and 5 actuated joints as can be seen in Figure 2.1. This results in a manipulator which can move in 5 degrees of freedom during different kinds of tasks. A gripper is attached to the last joint which consist of two fingers which allows the youBot to grasp small objects.

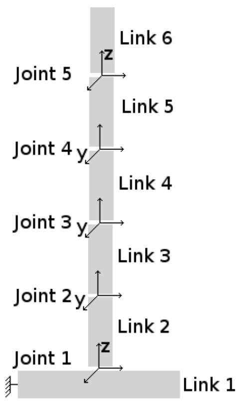

Figure 2.1: On the left the KUKA youBot and on the right a schematic representation (Dresscher, 2011). Joints 1 and 5 can freely rotate around the z-axis and the other joints operate around the y-axis.

2.1.1 Dynamic Model of the KUKA youBot arm

Screw theory (Stramigioli and Bruyninckx, 2001) is used to create a model of the rigid body dynamics. This theory states that the motion of rigid body can be represented by a rotation (ω) and a translation (v) along the same axis. These two velocities can be combined in one vector called a Twist: $T = \binom{\omega}{v}$. The Twist can be considered as the velocity of a rigid body, while the Wrench can be seen as the force exerted on the body. The Wrench, $W = \binom{\tau}{F}$, consist of torques (τ) and forces (F). In Equation 2.1 is shown the wrench balance which represents the inertia effect of the rigid body. In this equation I^k is the inertia of the rigid body and P the momentum screw, the momentum of a rigid body. $T_a^{k,0}$ is the Twist from coordinate frame a to inertial frame 0, expressed in coordinate frame k.

$$I^k \dot{T}_a^{k,0} = \begin{pmatrix} \tilde{P}_\omega^k & \tilde{P}_v^k \\ \tilde{P}_v^k & 0 \end{pmatrix} T_a^{k,0} + (W^k)^T \tag{2.1}$$

In this equation different coordinate frames are considered. k is representing the principle inertia frame, a represents the body frame and 0 is the inertial frame. During the derivation of the model coordinate changes will be required to be able to have physical correct kinematic relations. In the equations (2.2) to (2.5) will be shown how to do a coordinate transformation for Twists and Wrenches. To do this transformation a homogeneous matrix H_i^j is needed. This matrix represents the position of a frame i with respect to frame j. With p_i^j the translational component and R_i^j the rotational component, which is the change of rotation from body i to j.

$$\boldsymbol{H}_i^j = \begin{pmatrix} \boldsymbol{R}_i^j & \boldsymbol{p}_i^j \\ \boldsymbol{0} & 1 \end{pmatrix} \tag{2.2}$$

Using a twist in matrix form, $\tilde{\boldsymbol{T}}$, the following equation shows a coordinate transformation of twist $\tilde{\boldsymbol{T}}_k^{j,l}$ from frame i to j.

$$\tilde{\boldsymbol{T}}_k^{j,l} = \boldsymbol{H}_i^j \tilde{\boldsymbol{T}}_k^{i,l} \boldsymbol{H}_j^i \tag{2.3}$$

From this it can be derived that a coordinate change for Twists in vector form can be done using an adjoint of the homogeneous matrix. This is shown in the following equation:

$$\boldsymbol{T}_k^{j,l} = \boldsymbol{Ad}_{\boldsymbol{H}_i^j} \boldsymbol{T}_k^{i,l} \quad \text{with} \quad \boldsymbol{Ad}_{\boldsymbol{H}_i^j} = \begin{pmatrix} \boldsymbol{R}_i^j & 0 \\ \boldsymbol{p}_i^j \boldsymbol{R}_i^j & \boldsymbol{R}_i^j \end{pmatrix} \tag{2.4}$$

Due to power continuity, the coordinate transformation of a wrench is as follows:

$$(\boldsymbol{W}^i)^T = \boldsymbol{Ad}_{\boldsymbol{H}_i^j}^T (\boldsymbol{W}^j)^T \tag{2.5}$$

Using bond-graphs the above derived equations can be used within the dynamical model. Bond-graphs use the exchange of energy between different rigid bodies to model their behaviour. By using bond-graphs it is possible to model the relation between the different links and joints of the robot which also can be easily reused in other parts of the model, for the other link joints pairs. As the relation between twists and wrenches is power continues a transformer (*TF*) element can be used to represent the coordinate change. First the bond-graph representation of a link will be given. This model is created using 3 different frames:

- The Body fixed frame j in the previous joint, fixed to body of the previous link
- The Body fixed frame i in the next joint, fixed to body of current link
- The principle inertia frame k

Using these frames the model of the link is shown in Figure 2.2. In this figure the *TF* and *MTF* elements are used to change coordinates as discussed. In the upper part of the figure the mass and inertia of the link is modelled in the inertia frame, also the gyroscopic effects are added with the *MGY* element. This summation can also be seen in Equation 2.1. The effect of the gravitational force is modelled by adding an mass-dependant force represented by an effort source (*Se*).

The links are attached to each other with active rotational joints, the bond-graph model of such a joint is shown in Figure 2.3. As in the case of the link the, *TF* and *MTF* element are used for the coordinate transformation. Furthermore, a *C*-element and an *R*-element are used to constrain the motion in the directions other that the axis of rotation where the actuator is placed. A part of the total model can be seen in Figure 2.4. This figure depicts the first two links and joint, the bonds directed toward the joint are representing the motor actuation.

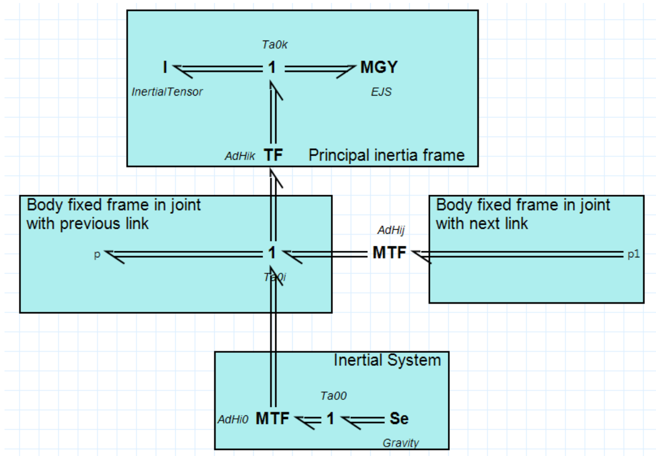

Figure 2.2: Bond-graph model of a link in the KUKA youBot

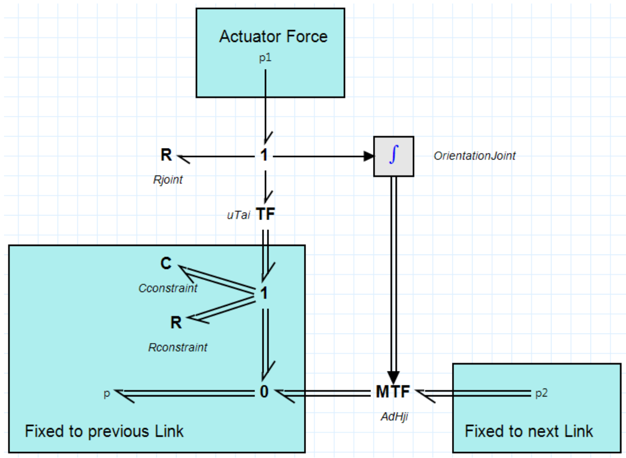

Figure 2.3: Bond-graph model of a joint in the KUKA youBot

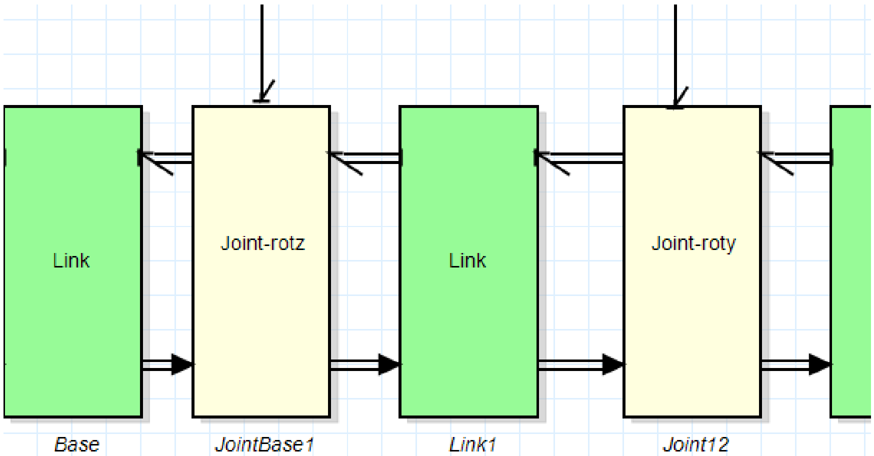

Figure 2.4: The first two links and joints of the total model of the KUKA youBot.

2.2 Impedance Control

This section briefly discusses the standard impedance control scheme which was the basis of the proposed safety aware controller design. In most cases of control engineering the position of an object or a force exerted on an object are controlled separately. But these are control actions used when there is no dynamic interaction with the environment. In case that this interaction is required, another type of controller is best used. There are commonly two controller types which are used for this dynamical interaction: Admittance control or Impedance control. With admittance control, the velocity of a dynamical system will be regulated by measuring the force and with impedance control the force will be controlled by measuring the velocity. In case an interaction has to be performed with the surrounding environment, the environment is generally considered as an admittance (Ferretti et al., 2004; Hogan, 1985). Because the environment is seen as an admittance, an impedance controller should be used for the manipulator. A schematic representation of an impedance controller in shown in Figure 2.5. In this figure, it is seen that the position is not directly given to the system, but via a spring and damper. This ensures closed loop stability of the system for all positive gains (Tadele et al., 2013).

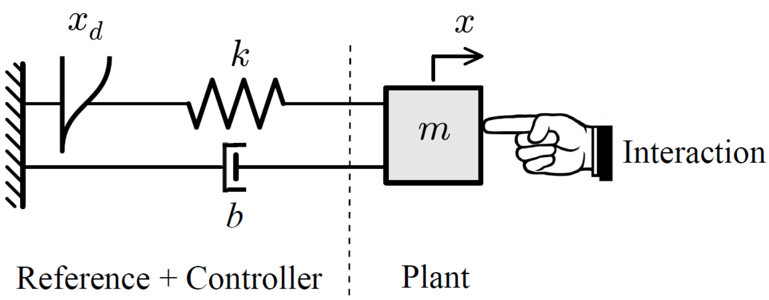

Figure 2.5: Example of an implemented impedance controller for 1DOF

Mathematically, the impedance controller for a 1 DOF system will expressed as is shown in Equation 2.6. Equation 2.7 give the dynamic equation for a controlled moving mass as show in Figure 2.5.

$$F_c = k(x_d - x) - b\dot{x} \tag{2.6}$$

$$F_c + F_{ext} = m \cdot \ddot{x} \tag{2.7}$$

The multidimensional extension of the impedance controller shown in Figure 2.6 is given mathematically as shown in Equation (2.8). In this equation $\boldsymbol{M}(\boldsymbol{q})$ is the inertia matrix, $\boldsymbol{C}(\boldsymbol{q}, \dot{\boldsymbol{q}})$ the Coriolis and centrifugal terms, $\boldsymbol{G}(\boldsymbol{q})$ the gravitational forces, $\boldsymbol{F}(\boldsymbol{q}, \dot{\boldsymbol{q}})$ the frictional forces and $\boldsymbol{\tau}$ represents the actuator forces.

$$\boldsymbol{\tau} = \boldsymbol{M}(\boldsymbol{q})\ddot{\boldsymbol{q}} + \boldsymbol{C}(\boldsymbol{q}, \dot{\boldsymbol{q}})\dot{\boldsymbol{q}} + \boldsymbol{G}(\boldsymbol{q}) + \boldsymbol{F}(\boldsymbol{q}, \dot{\boldsymbol{q}}) \tag{2.8}$$

The previously given dynamics are defined in joint space, however to accomplish tasks successfully, a cartesian space controller described in the operational space is more convenient. The dynamic equations of this controller are given in (2.9) to (2.12). $\tilde{\boldsymbol{m}}^t$ represents the torque component of the wrench $(\boldsymbol{W}^t)^T$ exerted on the spatial spring K. The linear forces of this wrench are represented as $\tilde{\boldsymbol{f}}^t$, where $as()$ is an operator used to obtain the skew-symmetric part of a square matrix. The co-stiffness matrices $\boldsymbol{G}_t, \boldsymbol{G}_c, \boldsymbol{G}_o$ are used as parts of the spatial spring K and represent the symmetric translational, coupling and rotational stiffness respectively. Transforming the wrench to the inertial reference frame Ψ_0 it can be used in Equation (2.12) which represent the impedance controller in cartesian space. $\hat{\boldsymbol{C}}(\boldsymbol{q}, \dot{\boldsymbol{q}})$ and $\hat{\boldsymbol{G}}(\boldsymbol{q})$ are used to compensate for Coriolis, centrifugal and gravitational forces. The damping parameters b_n are used in the diagonal matrix $\bar{\boldsymbol{B}}$. For a more detailed elaboration, pleas refer to Tadele et al. (2014b)

With these short introductions to impedance controllers the proposed safety aware impedance controller can be explained next in the following section.

$$\tilde{\boldsymbol{m}}^t = -2as(\boldsymbol{G}_o\boldsymbol{R}_t^d) - as(\boldsymbol{G}_t\boldsymbol{R}_d^t\tilde{\boldsymbol{p}}_t^d\tilde{\boldsymbol{p}}_t^d\boldsymbol{R}_t^d) - 2as(\boldsymbol{G}_c\tilde{\boldsymbol{p}}_t^d\boldsymbol{R}_t^d) \tag{2.9}$$

$$\tilde{\boldsymbol{f}}^t = -\boldsymbol{R}_d^t as(\boldsymbol{G}_t\tilde{\boldsymbol{p}}_t^d)\boldsymbol{R}_t^d - as(\boldsymbol{G}_t\boldsymbol{R}_d^t\tilde{\boldsymbol{p}}_t^d\boldsymbol{R}_t^d) - 2as(\boldsymbol{G}_c\boldsymbol{R}_t^d) \tag{2.10}$$

$$(\boldsymbol{W}^0)^T = \boldsymbol{Ad}_{\boldsymbol{H}_0^n}^T(\boldsymbol{W}^t)^T \quad \text{with} \quad \boldsymbol{W}^t = [\boldsymbol{m}^t \; \boldsymbol{f}^t] \tag{2.11}$$

$$\boldsymbol{\tau} = \boldsymbol{J}^T(\boldsymbol{q})\boldsymbol{W}^0 - \bar{\boldsymbol{B}}\dot{\boldsymbol{q}} + \hat{\boldsymbol{C}}(\boldsymbol{q}, \dot{\boldsymbol{q}}) + \hat{\boldsymbol{G}}(\boldsymbol{q}) \tag{2.12}$$

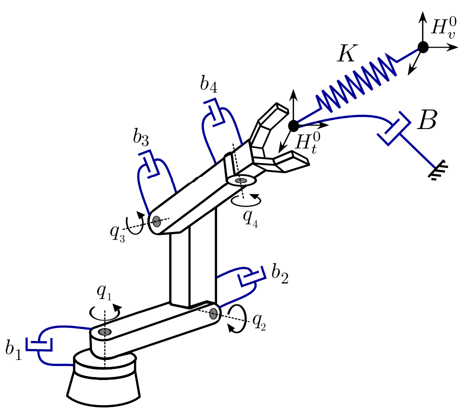

Figure 2.6: Multiple DOF implementation of the impedance controller (Tadele et al., 2014a). Compliance is added with a spatial spring defined as K and the damping is introduced with a spatial damper B or joint space damper b_n

2.3 Safety aware impedance controller

As discussed in the introduction, the safety aware impedance controller proposed by Tadele et al. (2014b) uses the energy and power of the manipulator to obtain a compliance behaviour that is acceptable to be used within domestic areas. With the addition of a passive implementation an inherently stable controller is obtained. Within this section the theory used to design the controller will be explained. First the controller for one degree of freedom will be explained, followed by the explanation of the multiple degree of freedom controller. To be able to safely interact with the environment this controller limits the power and energy of the used manipulator. These two limits will be obtained by changing the damping and stiffness parameters of an impedance controller. The stiffness constant of the impedance controller is used to limit the total energy of the manipulator as shown in Equation 2.13. The total energy is obtained by adding up the estimated kinetic and estimated potential energy of the system, given in Equation 2.14. The maximum energy is the energy that a human body can tolerate without getting severe injuries. Next to the maximum energy, the desired position x_d , actual position x and the velocity $\dot{x}$ of the manipulator are used with the mass m. The maximum stiffness coefficient k_0 depends on the performance requirements of the system.

$$k = \begin{cases} k_0 & \text{if} \quad E_{tot} \leq E_{max} \\ \dfrac{2E_{max} - m\dot{x}^2}{(x_d - x)^2} & \text{otherwise} \end{cases} \tag{2.13}$$

$$E_{tot} = \frac{1}{2}kx_e^2 + \frac{1}{2}m\dot{x}^2 = E_{pot} + E_{kin} \quad \text{with} \quad x_e = x_d - x \tag{2.14}$$

To limit the amount of power that the manipulator can exert during an uncontrolled impact, the power flow to the used actuators can be regulated. This power flow is given in Equation 2.15 and can be regulated by using the damping parameter b. This damping parameter will be calculated as shown in Equation 2.16. In this equation $P_{c_{max}}$ is the maximum power that a human body can tolerate before getting injuries. b_0 has to be chosen such that the system has a acceptable damping behaviour when no power limit is active.

$$P_c = (k(x_d - x) - b\dot{x})\dot{x} \tag{2.15}$$

$$b = \begin{cases} b_0 & \text{if} \quad P_c \leq P_{c_{max}} \\ \dfrac{k(x_d - x)\dot{x} - P_{c_{max}}}{\dot{x}^2} & \text{otherwise} \end{cases} \tag{2.16}$$

Due to this parameter regulation, the total energy in the system and the power flow have to be monitored continuously during movement of the manipulator. This means that when the total energy of the system will exceed the maximum energy, the controller has to become more compliant. In the same way, extra damping will be added when the actuator uses more power than the given maximum value. After obtaining the right parameters the impedance controller given in Equation 2.17 is used. A problem with this impedance controller is that the passivity of the system will be affected while using a variable impedance controller. Which is true in this case because the parameters b and k can be changed in time. To still have a guaranteed stability this, an energy tank based implementation will be used, where the controller will be used as a power flow modulator between an energy storage tank and a plant. Such a system is shown in Figure 2.7. In this figure C_S is used as the energy tank which behaves as an energy storage spring with stiffness constant k=1. MT is a transmission element with a variable transmission ratio u which is calculated using the computational unit CU. This transmission ratio can be obtained by using the controller output force F_c in Equation 2.17 and the state s of the spring C_S which is equal to the output force. The relation between these two variables are shown in Equation 2.19. This relation is derived by the port Hamiltonian equations as shown in Tadele et al. (2014b) and given in (2.18), with p the momentum of the plant and $\dot{x}$ the velocity of the plant. $H(C_S) = \frac{1}{2}s^2$ is the potential energy in the tank and ϵ the minimum amount of energy which has to be available in the tank to have power flow from the tank towards the manipulator. $P_c = F_c\dot{x}$ is the power flowing from the controller to the plant.

$$F_c = k \cdot (x_d - x) - b \cdot \dot{x} \tag{2.17}$$

$$\begin{pmatrix} \dot{s} \\ \dot{p} \end{pmatrix} = \begin{pmatrix} 0 & u \\ -u & 0 \end{pmatrix} \begin{pmatrix} s \\ \dot{x} \end{pmatrix} \tag{2.18}$$

$$u_d = \begin{cases} 0 & \text{if } ((H(C_S) < \epsilon) \wedge (P_c < 0)) \\ \dfrac{-F_c}{s} & \text{otherwise} \end{cases} \tag{2.19}$$

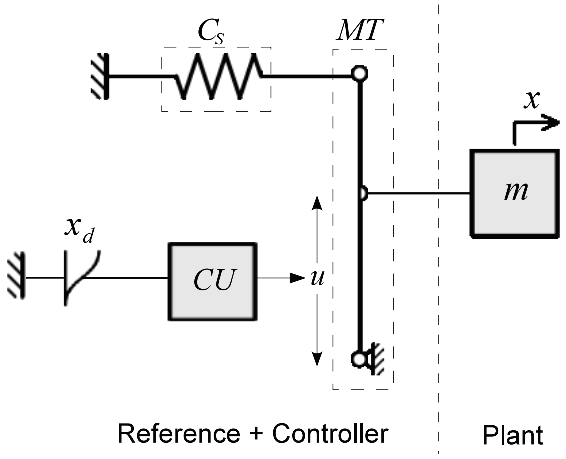

Figure 2.7: 1 DOF implementation of the prosed controller (Tadele et al., 2014b)

Because the manipulator that will be used during this project can move in 5 degrees of freedom, the controller should also be calculated for multiple degrees of freedom. For this case the same relations used above will be used, only instead of using an output force the joint torque τ_n will be used and the joint positions (q) and velocities ($\dot{q}$) will be used instead of the translational velocities and position. Next to the kinetic energy shown in Equation 2.20 also the sum of translational, rotational and coupling energies (2.21) is needed to calculate the total energy of the system (2.22). Where $\boldsymbol{T}(\boldsymbol{q}, \dot{\boldsymbol{q}})$ is representing the kinetic energy and $\boldsymbol{V_i}(\boldsymbol{R_t^d}, \boldsymbol{p_t^d})$ the sum of the potential energies. Assuming the potential energy of the manipulator due to gravity is cancelled by a compensator, the energy values in the system are given mathematically as Tadele et al. (2014b).

$$\boldsymbol{T}(\boldsymbol{q}, \dot{\boldsymbol{q}}) = \frac{1}{2}\dot{\boldsymbol{q}}^T \boldsymbol{M}(\boldsymbol{q})\dot{\boldsymbol{q}} \tag{2.20}$$

$$\boldsymbol{V_i}(\boldsymbol{R_t^d}, \boldsymbol{p_t^d}) = \boldsymbol{V_t}(\boldsymbol{R_t^d}, \boldsymbol{p_t^d}) + \boldsymbol{V_o}(\boldsymbol{R_t^d}) + \boldsymbol{V_c}(\boldsymbol{R_t^d}, \boldsymbol{p_t^d}) \tag{2.21}$$

$$\boldsymbol{E_{tot_i}} = \boldsymbol{T}(\boldsymbol{q}, \dot{\boldsymbol{q}}) + \lambda \cdot \boldsymbol{V_i}(\boldsymbol{R_t^d}, \boldsymbol{p_t^d}) \tag{2.22}$$

To limit the output energy the co-stiffness matrices $\boldsymbol{G}_x$ given in (2.9) and (2.10) will be scaled with a scaling parameter λ and is formulated as:

$$\lambda = \begin{cases} 1 & \text{if } \boldsymbol{E}_{tot_i} \leq \boldsymbol{E}_{max} \\ \frac{\boldsymbol{E}_{limit} - \boldsymbol{T}(\boldsymbol{q},\dot{\boldsymbol{q}})}{\boldsymbol{V}_i(\boldsymbol{R}_t^d, \boldsymbol{p}_t^d)} & \text{otherwise} \end{cases} \tag{2.23}$$

$$\boldsymbol{G}_x = \lambda \cdot \boldsymbol{G}_{x_i}$$

$$\boldsymbol{P}_{\boldsymbol{c}_i} = \underbrace{(\boldsymbol{J}^T(\boldsymbol{q}) \cdot \boldsymbol{W}^0 - \beta \cdot \bar{\boldsymbol{B}}_{\boldsymbol{i}} \cdot \dot{\boldsymbol{q}})^T \cdot \dot{\boldsymbol{q}}}_{P_{c_m}} + \underbrace{\hat{\boldsymbol{G}}(\boldsymbol{q}) \cdot \dot{\boldsymbol{q}}}_{P_{c_{g}c}} \tag{2.24}$$

Using this scaling parameter the total energy will be less than the maximum energy that is derived to prevent injuries or damage to the environment. Also the power that will be transferred to the plant (2.24) will be limited to avoid dangerous situations, with P_{c_m} the motor driven power and $P_{c_g c}$ the power to compensate for gravitation. It will be limited by scaling the damping matrix $\bar{\boldsymbol{B}}_i$ with the parameter β. This parameter is given as:

$$\beta = \begin{cases} 1 & \text{if } P_{c_m} \leq P_{max} \\ \dfrac{(\boldsymbol{J}^T(\boldsymbol{q}) \cdot \boldsymbol{W}^0)^T \cdot \dot{\boldsymbol{q}} - P_{max}}{\dot{\boldsymbol{q}}^T \cdot \bar{\boldsymbol{B}}_{\boldsymbol{i}} \cdot \dot{\boldsymbol{q}}} & \text{otherwise} \end{cases} \tag{2.25}$$

$$\tag{2.26}$$

The above derived parameters will then result in a control torque $\boldsymbol{\tau}_c$ as shown in Equation (2.12).

Figure 2.8 shows the graphical interpretation of the multi degree of freedom formulation of the controller. In this figure is shown that each joint of the robot has its own storage tank CS and transmission ratio u. In this case a control unit CU will calculate the transmission ratio such that a proper controller action is performed. The transmission ratio will be calculated using Equation 2.27.

$$u_n = \begin{cases} 0 & \text{if } ((H(CS_n) < \epsilon) \wedge (P_n < 0)) \\ \dfrac{-\tau_n}{s_n} & \text{otherwise} \end{cases} \tag{2.27}$$

The design of the total controller that is shown above can be summarized in a multilayer structure as shown in Figure 2.9. Using this structure the output torques of the impedance controller in the motion layer will be evaluated in the following Safety and Passivity layer. Using this design a passivity based safety aware impedance controller is been obtained which is able to safely interact with its environment.

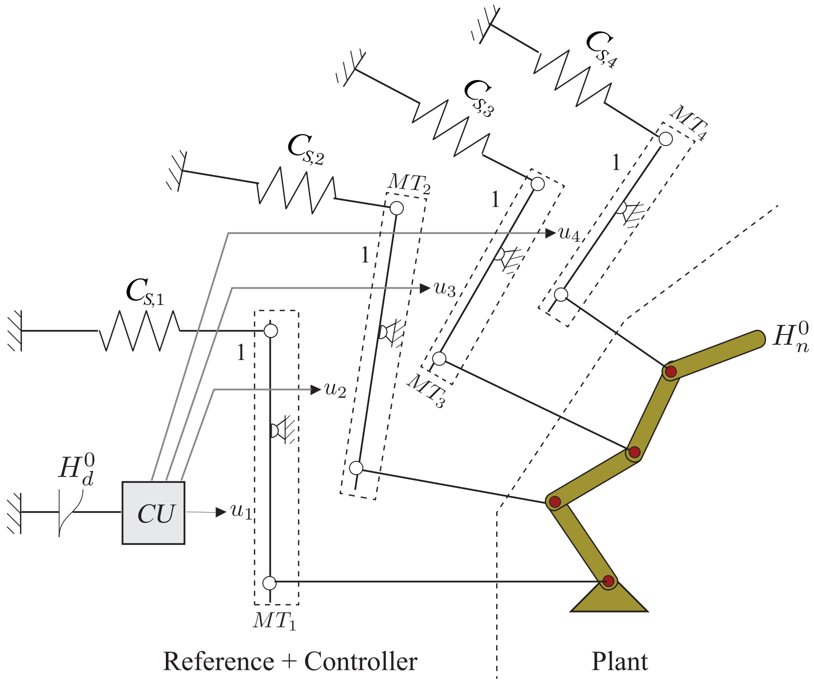

Figure 2.8: Multiple DOF implementation of the proposed controller (Tadele et al., 2014b)

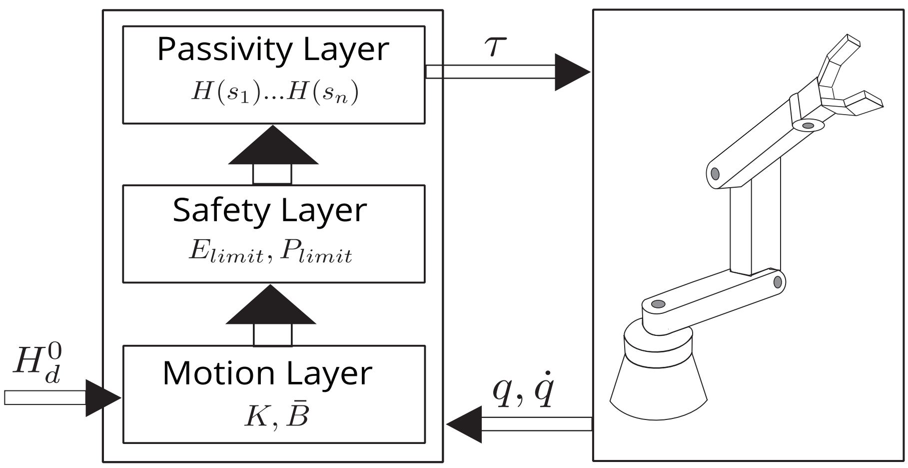

Figure 2.9: Layer structure of the proposed controller

3 Test Plan

3.1 Model used during testing

During the tests of the proposed controller the KUKA youBot model given in Brodskiy et al. (2013) and Frijnts (2014) is used. This model has been developed such that the robot can be controlled using a haptic device. The model is made available in 20sim (Controllab products, 2015) a simulation program which is able to simulate models that are using bond graphs. Figure 3.1 shows the used 20-sim implementation of the model and the controller. Within the *ArmPoseController* the commanded torque *Tc* and measured velocities and positions are checked such that they do not exceed given limits which can damage the KUKA youBot. Also the gravitation compensation *Tg* is included in this part of the model to keep the manipulator at the desired position. The communication between the controller and the KUKA youBot is performed using a real time software library OROCOS(Orocos Project, 2015). It is possible to convert 20-sim code to OROCOS components, which enables to use the same architecture as used in 20-sim. Therefore it is easy to add additional components when the same signals are used. A more detailed description of this software library and the conversion of 20-sim models can be found in Brodskiy et al. (2013) and Frijnts (2014).

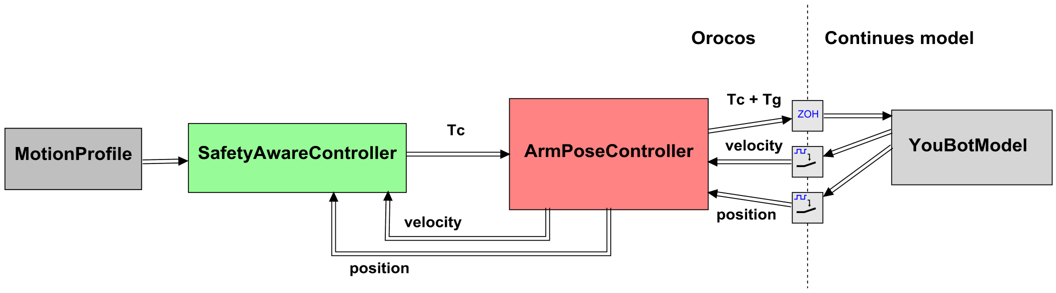

Figure 3.1: Schematic of the model implementation used during this project.

3.2 Test overview

The different tests will be performed in a sequential order. This means that first the results of the 1 DOF controller will be obtained and verified. After that an extra joint will be added in the control loop such that a multi degree of freedom test can be obtained. As last part all the joints will be added such that the total system can be evaluated. The proposed controller uses a multi layered architecture, as shown in Figure 3.2, that allows separate implementation and testing of the layers. With this the influence of the different layers can be tested. The implementation order will follow the numbers shown in Figure 3.2. First the motion layer with the impedance control will be implemented and tested in simulation. After this the passivity layer will be added such that it is possible to use the youBot at this stage. With this, the simulation results can be compared with the results obtained from the real system. If the robot is moving as expected, the third and last layer can be added. This last layer, the safety layer, contains the part of the proposed controller which limits the power and energy output.

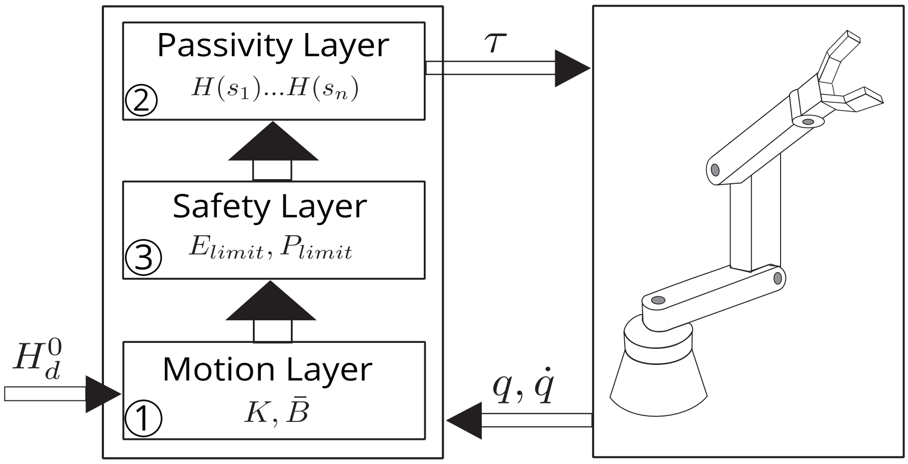

Figure 3.2: Layer structure of the proposed controller

3.3 Measurement plan

During the verification of the controller, three parts of the controller have to be evaluated, the performance, the stability of the system and the limitation of the energy and power. Besides these two parts of the controller also the performance of the whole system has to be taken into account. The measurements will be performed in a one degree of freedom configuration and in a multi degree of freedom configuration. In the following sections, the measurements are given which will be used to verify the controller and the total system.

3.3.1 Measuring the Safety limits

An important part of the controller is the safety limits which will be used for safe human interaction. The verification of this part will be done by measuring the stiffness and damping parameter which will be changed when the corresponding limitation will be exceeded. The controller is considered to be safe if the given limits will not be exceeded and the according parameters will change as expected.

- Value change of the stiffness parameter k, λ
- Value change of the damping parameter b, β

To test if the parameters will be changed when the maxima will be exceeded, the manipulator has to perform different tasks. These tasks will consist of following a predetermined path.. In Section 3.3.4 the three different motion types are explained. Because it should be possible to safely interact with the manipulator which uses the described controller, interaction will also be tested.

- Free motion trajectory
- Collision trajectory
- Interaction with environment or human

3.3.2 Measuring passivity/stability

An important requirement of any controller is a stable performance during its standard operation. Also the actuators of the joint should not be able to exert more power than asked. This can be investigated by measuring the following parts of the controller. The position of the manipulator can be used to see if it will converge to the setpoint. One of the design parameters of the controller is that using the energy based storage tank will result in a passive system. Therefore the state of this tank will be measured to see if it is decreasing during motion which means no extra energy is generated during motion.

- Position of the manipulator
- Available energy in tank

To meet several conditions the following test will be performed with the manipulator. These tests include a collision with a soft material and interaction with a human. During these tests the controller should have a compliant behaviour and will remain stable during any kind of interaction.

- Collision trajectory
- Interaction with environment or human

3.3.3 Performance

Also the performance of the total system is of importance because the given tasks should be performed within an acceptable error range. This performance will be mainly determined by the choice of the initial values of the stiffness and damping parameters. These parameters are chosen such that the impedance controller will have a minimum motion error. The performance of the controller will be measured using the following variables:

- position of end effector
- actuator current

The position of the manipulator will be used to obtain the motion error and finally the setpoint error. So to measure the free motion trajectory and a trajectory with a collision will be used. The actuator current will be used to get information about the applied torque on the manipulator.

3.3.4 Types of movement

To verify the controller that has been implemented, the robotic arm has to perform certain tasks. These tasks consist of following a pre-planned trajectory or holding a certain setpoint. Using these two tasks, the following 3 experiments can be formulated. The test can all be performed while moving in 1 degree of freedom and multiple degrees of freedom. If the tests are performed in 1 DOF, one joint will be active and the others will be keeping their initial position with active control. By adding a degree of freedom an additional joint will be activated.

Free movement

During free-motion the robotic arm will follow a given trajectory. During this control action the initial damping parameter b and stiffness coefficient k should be chosen such that it follows the trajectory with a low motion error. The total controller should change the parameters according the limitation of the power and energy usage. This change of parameters should not interfere with the primary task of following the trajectory.

Movement with collision

To know if the controller will not exceed the given conditions during an uncontrolled action, an object will be placed in the path of motion. This object will consist of a soft material such that the robot will not get damaged during the collision. It is expected that the system will change the stiffness constant to limit the energy that will be given to the object. Also the system has to remain stable due to the passivity layer. After the collision the manipulator should continue its path.

Human Interaction/ Environment Interaction

During the interaction with a human the system should be compliant such that the human user will not get injuries. During this phase the power and energy limits should also be respected. During the interaction the system should also remain stable to avoid dangerous situations. Afterwards the path or setpoint should be recovered under the given conditions. Next to interaction with a human also the interaction with the surroundings will be tested. Because in the future the controller will be used in domestic robotic manipulators the controller has also to be tested with these conditions. This can be done by moving the manipulator over a surface to mimic cleaning a table for example.

3.4 Test setup

In this section the test setup used during testing of the controller will be given. All the tests will be performed with the use of the arm of the KUKA-youBot. Before the tests will be done on the robotic arm itself it will be simulated. So it can already be tested if the manipulator will not exceed the maximum values, with can damage the robotic arm.

3.4.1 One DOF test

Figure 3.3 shows a 3D-model of the KUKA-youBot . In this figure the youBot is placed in an initial position which will be used to perform the 1DOF test. In this configuration the base joint will follow a given path. It is intended to obtain comparable results as shown in the research of Tadele et al. (2014b). The tests will be performed according to Section 3.3

Figure 3.3: 3D model KUKA youBot. (KUKA Laboratories, 2014)

For the test with a collision, a soft object will be placed in the manipulator's motion path. The object will prevent the robotic arm of moving further. A soft material will be chosen because the robot should not damage itself during collision. Also this soft material will represent the soft skin of a human. Figure 3.4 shows a graphical representation of this setup.

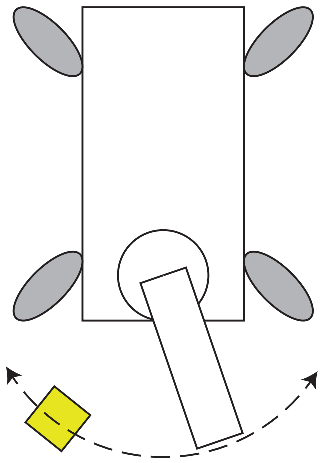

Figure 3.4: Collision trajectory test setup.

3.4.2 Multiple DOF tests

For the test with more than one active joint the same setup is used, as in the case of the 1 DOF measurements. The difference is that more than one joint will be active while following given path. Also the object for collision will be placed in different positions so other configurations can be tested.

4 Controller Design

In this chapter the control design of the used controller is explained. The control parameters for the one degree of freedom impedance controller will be calculated for the controlled joints 1 and 4 of the KUKA youBot. In the last section of this chapter the use of a friction compensation controller will be discussed.

4.1 One Degree of Freedom Controller design

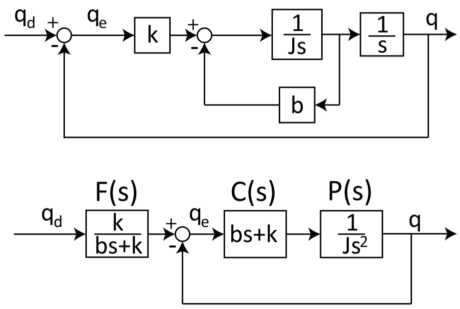

Figure 4.1: Block diagram of the controlled system

To obtain the controller parameters of the one degree of freedom impedance controller the block diagrams in Figure 4.1 will be used. The first diagram is obtained by representing the controlled system into a block diagram using Equation 4.1. Where T_c is the controller output and J the inertia of the manipulator. The control parameters k and b have to be chosen properly to obtain desired behaviour of the total controlled system.

$$T_c = k \cdot (q_d - q) - b \cdot \dot{q} = k \cdot q_e - b \cdot \dot{q} \tag{4.1}$$

To derive the values of k and b the first block diagram will be changed in a representation with a single controller $C(s)$ and plant $P(s)$ and unity feedback. This representation is shown in the lower part of Figure 4.1. Using the derivation of the control parameters in Tadele et al. (2014a), the formulation of the control parameters in Equation 4.2 and Equation 4.3 are obtained.

$$k = \frac{4 \cdot \zeta \cdot J_{end\_eff}}{e_{max}^2} \cdot \omega_{max}^2 \tag{4.2}$$

$$b = 2\zeta \cdot \sqrt{k \cdot J_{end\_eff}} \tag{4.3}$$

To obtain the controller parameters, first the values of the three parameters will be chosen based on the desired performance of the total system. From these parameters the maximum rotational velocity is defined as ω_{max}, the maximum error as e_{max} and ζ as the damping ratio. The values of these three parameters depend on the performance criteria of the system. In this case the values are chosen as shown in Equations (4.4) to (4.6).

$$\text{Joint 1}: \ \omega_{max} = 0.4 \ \{\text{rad/s}\} \quad \text{Joint 4}: \ \omega_{max} = 0.4 \ \{\text{rad/s}\} \tag{4.4}$$

$$\text{Joint 1}: \ e_{max} = 0.1 \ \{\text{rad}\} \quad \text{Joint 4}: \ e_{max} = 0.05 \ \{\text{rad}\} \tag{4.5}$$

$$\text{Joint 1}: \ \zeta = 0.7 \quad \text{Joint 4}: \ \zeta = 0.7 \tag{4.6}$$

From all the parameters in Equation 4.2 only the end effector inertia J_{end_eff} is still unknown. This inertia can be obtained by using the dynamical model in Figure 4.2. In this model the inertia of the manipulator is given as J_{man} and the inertia of the motor with J_m. A gearbox with a gearratio i connects the motor and the corresponding link of the KUKA youBot. Furthermore the actuated torque is derived with a current controller, where the torque constant k_m is used to obtain the corresponding torque. The KUKA youBot has position sensors which can be used during control.

In Figure 4.3 is given the reduced dynamical model of the previous given system. This reduction is done by removing the transmission of the gearbox by dividing the Torque T_c and motor inertia J_m by the gearbox ratio i. The end-effector inertia will be calculated using Equation 4.7. To have a proper model reduction the motor driven torque T_{act} should also be divided by i which results in a torque as shown in Equation 4.8. Because it is seen that the applied torque of the controller will result in a corresponding motor torque, there is no need to change the output torque of the controller.

$$J_{end\_effector} = J_{man} + \frac{J_m}{i^2} \tag{4.7}$$

$$T_{act} = \frac{T_c}{i} \tag{4.8}$$

Using the calculated end-effector inertia and the other given parameters an initial stiffness and damping parameter are obtained as $k_0 = 11.829\{\mathrm{N\,m\,s/rad}\}$ and $b_0 = 2.9572\{\mathrm{N\,m\,s/rad}\}$ respectively for manipulator joint 1. For joint 4 the control parameters are: $k_0 = 5.9898\{\mathrm{N\,m\,s/rad}\}$ and $b_0 = 0.7477\{\mathrm{N\,m\,s/rad}\}$

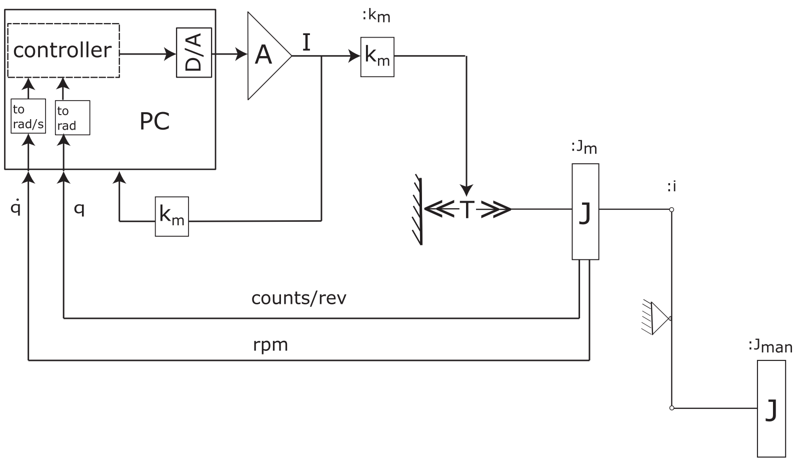

Figure 4.2: System diagram of safety aware controller with the KUKA youBot arm as manipulator. k_m torque constant, J_m motor inertia, i transmission ration

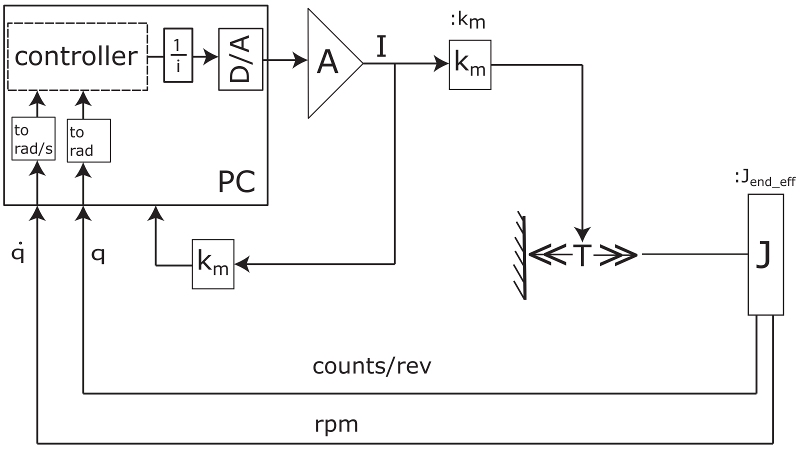

Figure 4.3: Reduced system diagram of safety aware controller with the KUKA youBot arm as manipulator. k_m torque constant, J_{end_eff} end effector inertia, i transmission ration

To analyse the obtained control parameters a bodediagram of the openloop transfer is obtained and shown in Figure 4.4. The analysis will be shown for joint 1, since for joint 4 simular results will be obtained. From the bodediagram in Figure 4.4 can be seen that the controlled system is intrinsic stable, because the phase difference will never be bigger as 180°. This is also seen in Figure 4.5b which shows the pole-zero plot of the closed loop system. The closed loop poles are placed on the position according to the damping ratio of 0.7.

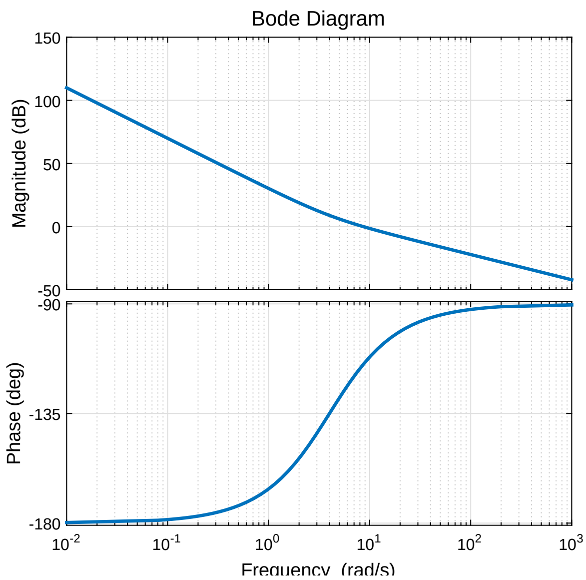

Figure 4.4: Bodediagram of the loop transfer with the 1DOF controller shown in Figure 4.1 using the parameters of joint 1

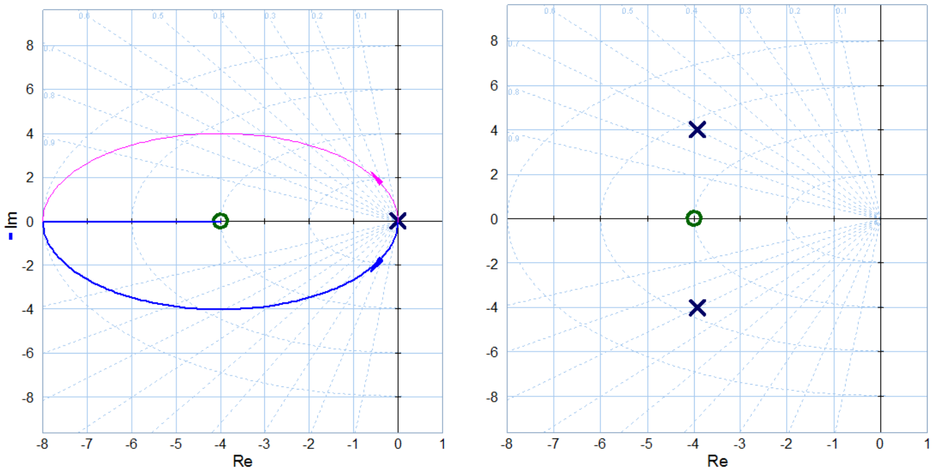

(a) Open loop poles

(b) Closed loop poles

Figure 4.5: Pole zero plots of the 1DOF impedance controller using the system shown in Figure 4.1. In (a) are shown the openloop poles with the corresponding root loci. (b) shows the closed loop poles of the initial configuration

According to Section 2.3 the parameters of the impedance control will change when an energy limit and/or power limit is reached. This will cause that the location of the poles of the closed loop system will change. In case the energy limit is reached, the value of the stiffness constant k will change according to Equation 4.2. Changing the stiffness will cause the poles to move along the root loci shown in Figure 4.5a and changing the damping ratio ζ effectively. This will result in a change of the total performance of the system. To have acceptable behaviour while keeping the energy limit the safety aware controller will be changed such that the damping parameter is changed together with the stiffness parameter. This change is shown in the code block below. This code is used within the controller to meet the safety criteria and is implemented according to Section 2.3.

In case of power limitation both parameters will not be changed simultaneously because this will counteract the safety performance of the system. For limiting the power the damping parameter b of the controller will be increased to keep the power output constant. When the stiffness constant k will also be changed to keep the damping ratio ζ constant, it will result in a system which is more stiff. Which means that during interaction or collision safety will no be guaranteed.

```
Kc = k0;   // Control stiffness
Bc = b0;   // Control damping
Jtot = Jend_effector;


E = 0.5 * (( Kc*qe^2 + Jtot*qdot^2)); //Energy of the system

if E > Emax then
        Kc = (2*Emax - Jtot*qdot^2)/(qe^2);
        Bc = 2*zeta*sqrt(Kc*Jtot);
end;

tc = (Kc*(qe)-Bc*qdot); //Impedance controller equation
Pc = tc*qdot;    //Power flow from controller to plant

if Pc > Pmax then
                Bc = (Kc * qe)/qdot - (Pmax)/(qdot^2);
end;

Tc = (Kc*qe - Bc*qdot)    //Final impedance controller equation
```

Listing 4.1: Part of the code used in the safety aware impedance controller

4.2 Friction compensation

In this chapter the design and use of a controller for compensation of friction is explained. First the friction in joint 1 and 4 of the manipulator will be obtained, these acquired friction profiles will be used in the controller. After this section, the achieved profiles will be evaluated using the 20sim model of the KUKA youBot. Finally different possible implementations of the controller will be given and discussed.

4.2.1 Obtaining friction profile

To compensate for energy loss during motion due to friction, a controller will be designed. This controller will use a measured friction profile to add the torque needed to compensate for the available friction.

To obtain the friction profile within the joints of the KUKA youBot, measurements of the torque and velocity are used. These measurements are shown in Figure 4.6, where the crosses representing the measurement data. The obtained profile can be divided into three different regions:

- $v < 0$: Friction during negative velocity consisting of Coulomb and viscous friction.
- $v > 0$: Friction during positive velocity consisting of Coulomb and viscous friction.
- $v = 0$: Friction due to stiction.

Each region is represented with a formula to describe the average friction in that region. These formulas are shown in Equations (4.9) and (4.10). To avoid a discontinues system, or by having multiple possible solutions at the same velocity, a curve with a high slope is used around zero velocity. The slope in this region is chosen such that the profile is high enough to approximate the stick behaviour, but not too high such that an instantaneous change occurs between two regions.

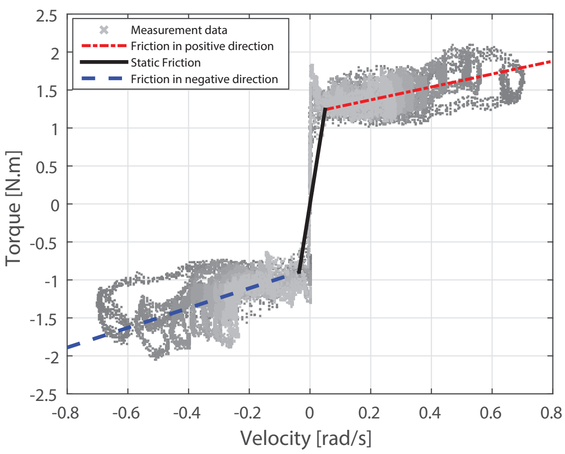

(a) Joint 1

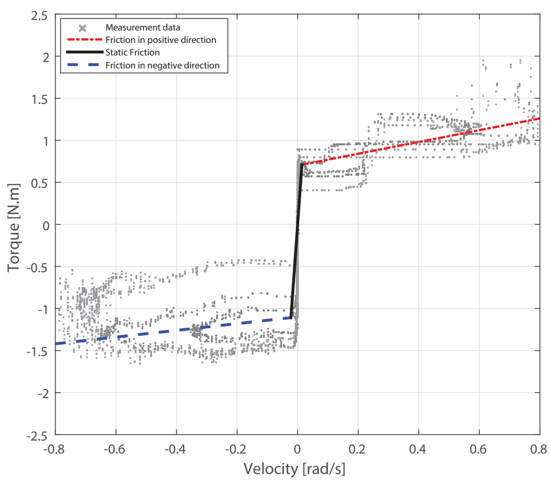

(b) Joint 4

Figure 4.6: Friction profile of Joint 1 and Joint 4 of the KUKA youBot

$$\text{Joint 1}: \quad \tau_{friction} = \begin{cases} 1.3 \cdot \dot{q} - 0.85 & \text{if} \quad \dot{q} < -0.0357 \text{ \{rad/s\}} \\ 0.95 \cdot \dot{q} + 1.2 & \text{if} \quad \dot{q} > 0.0497 \text{ \{rad/s\}} \\ 25 \cdot \dot{q} & \quad\;\;\;\; \text{Otherwise} \end{cases} \tag{4.9}$$

$$\text{Joint 4}: \quad \tau_{friction} = \begin{cases} 0.4 \cdot \dot{q} - 1.1 & \text{if} \quad \dot{q} < -0.0222 \text{ \{rad/s\}} \\ 0.7 \cdot \dot{q} + 0.7 & \text{if} \quad \dot{q} > 0.0142 \text{ \{rad/s\}} \\ 50 \cdot \dot{q} & \quad\;\;\;\; \text{Otherwise} \end{cases} \tag{4.10}$$

4.2.2 Evaluation

For evaluating the retrieved friction profile, the dynamical model presented in in Section 2.1.1 of the KUKA youBot will be used. The friction profiles in Equation 4.9 and Equation 4.10 will be added as friction in the corresponding joint of the robot.

Figure 4.7 shows the torque profiles is used to evaluate the obtained friction models. These profiles are commanded to the KUKA youBot without using a feedback loop such that the behaviour for input torques can be analysed.

From the measurements in the given figures can be seen that the actual torque sent to the motors differs from the torque which is requested. This difference is due to the current controller which is available in the KUKA youBot, which is not designed optimally. However, a remedy is not available, therefore this torque profile can be used during evaluation of the friction profile.

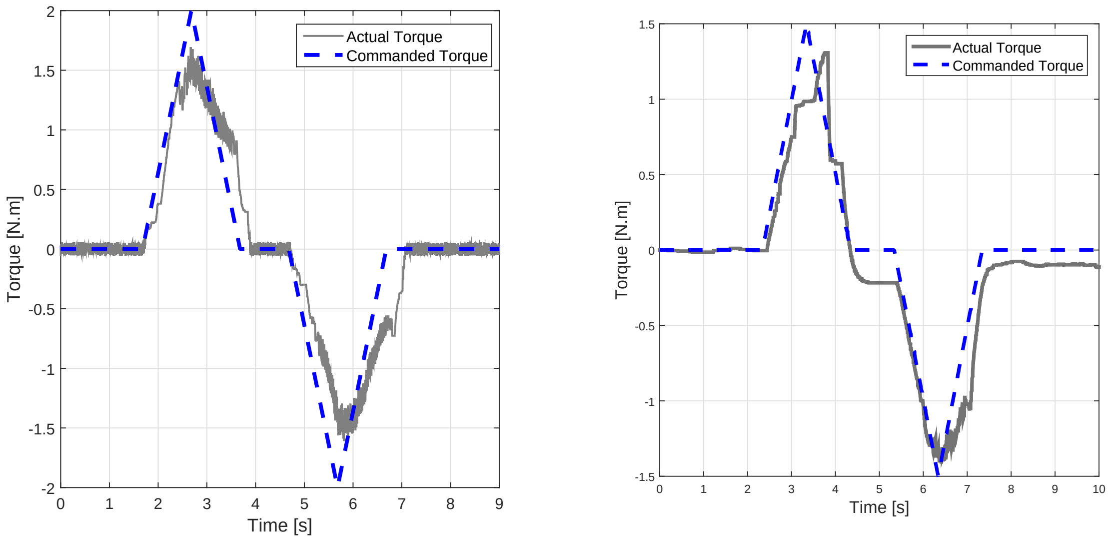

(a) Joint 1

(b) Joint 4

Figure 4.7: Commanded and Measured torque of Joint 1 and Joint 4 of the KUKA youBot.

Figure 4.8 shows the obtained position and velocity corresponding to the torque exerted by the motor in the joint. These measurements show that the friction is direction dependent which is expected considering the obtained formulas in Equations (4.9) and (4.10).

Using the measured torque the position and velocity of the corresponding joint in the 20sim model are obtained. These measurements are shown in Figure 4.9. Comparing the obtained results with the ones from the experiments it can be seen that the both figures show corresponding shapes with different amplitudes. Because the used friction profile is an approximation of the real friction the results are expected to be different. According to these results it will be decided that the given friction representation can be used in a controller to compensate for the available friction.

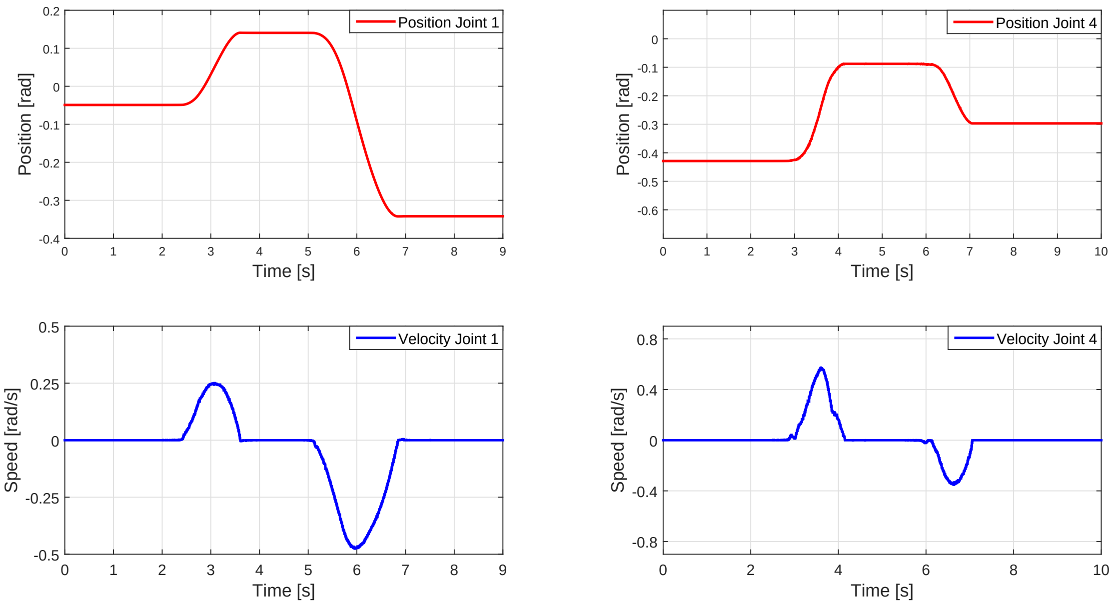

(a) Joint 1 **(b)** Joint 4

Figure 4.8: Measured angular velocity and position during experiment with Joint 1 and Joint 4 of the KUKA youBot using the corresponding torque input in Figure 4.7

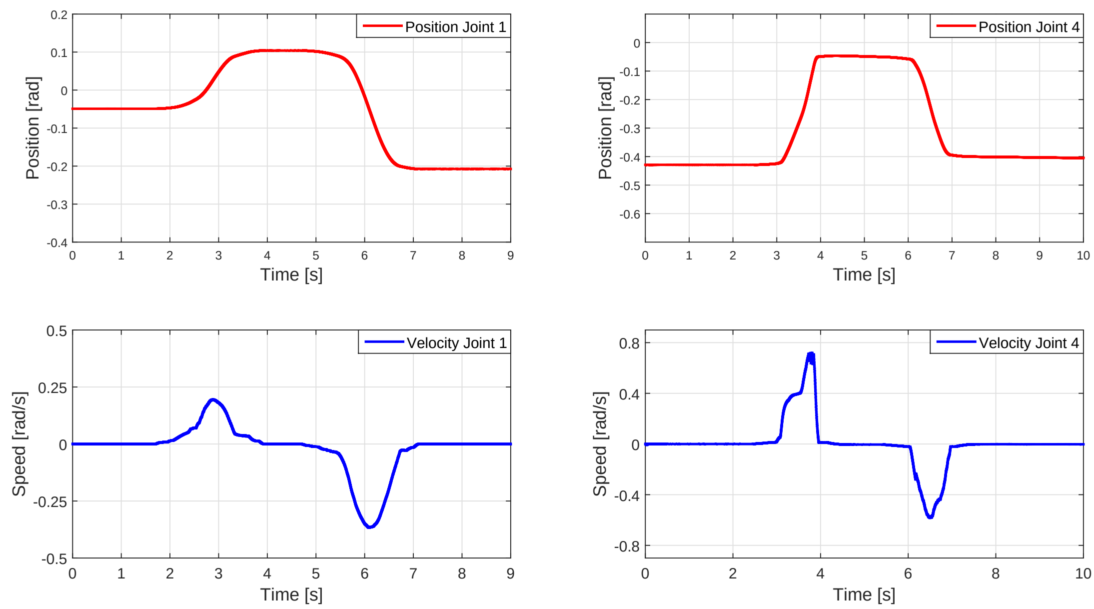

(a) Joint 1 **(b)** Joint 4

Figure 4.9: Measured angular velocity and position during simulation with Joint 1 and Joint 4 of the KUKA youBot model. The actual torque output of Figure 4.7 is used as input of the corresponding joint.

4.2.3 Implementation of the friction compensation controller

There are a few possibilities to implement a controller to compensate for friction. Figure 4.10 shows a plant compensation controller which uses the current velocity of the plant to compensate for the friction. An advantage to use this implementation is that by using this controller the velocity of the plant can be controlled using the safety aware impedance controller. Using this implementation the controller sees an augmented plant which behaves as a plant without friction. The same method is used to compensate for gravitation where the gravitational component depends on the orientation of the manipulator and is also compensated with a feedback loop. A draw back to this implementation is that the controlled system is not passive any more.

Another implementation is shown in Figure 4.11. This figures shows the use of a feed forward controller which uses the expected velocity $\dot{q}_d$ of the desired motion profile to compensate for the available friction. A disadvantage of using this controller is that the system is not passive and that during collision/interaction the feed forward controller will still generate a torque output to follow the motion profile.

A third possible option is to add the compensation of the friction within the safety and passivity layer of the prosed controller shown in Figure 2.9. This will results in a total controller which is still passive and able to use the desired safety limits.

Due to timing issues it was not possible to change the proposed controller to use with the third option, therefore it is chosen to use the configuration shown in Figure 4.10 which is still able to meet the safety requirement but not the passivity. But the loss of passivity is not a problem because experiments will be performed in a known environment.

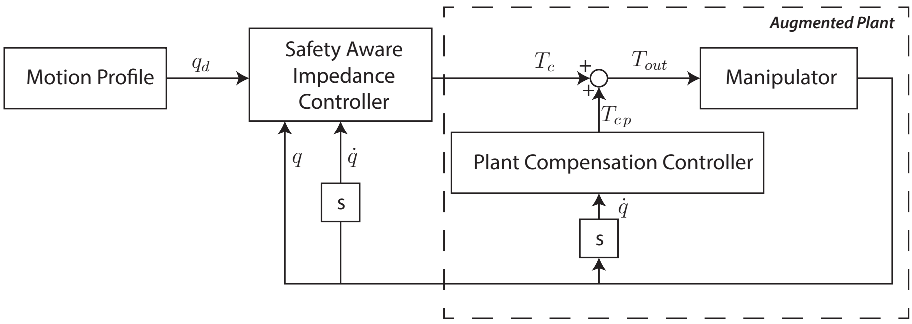

Figure 4.10: Implementation of the plant compensation controller with the safety aware impedance controller

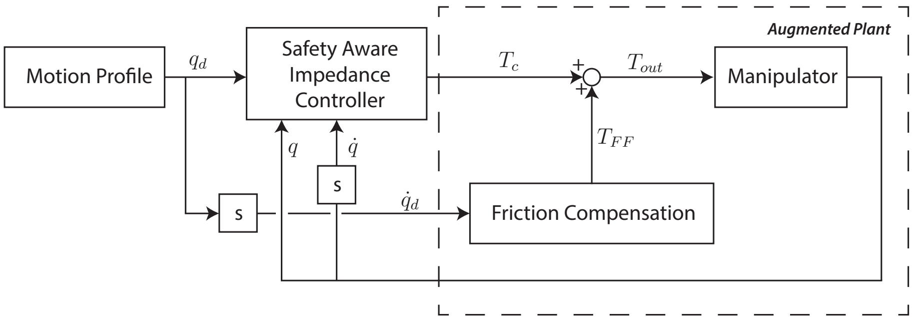

Figure 4.11: Implementation of the Feed Forward controller with the safety aware impedance controller

5 Results

Within this chapter the results obtained during the experiments will be given. The chapter is devided into different sections. First the results obtained with the 1DOF safety aware impedance controller in joint space is given. Following this, the results obtained with the controller in cartesian space will be presented. The obtained results are presented such that it is clear which values are obtained. Therefore it should be noted that while comparing different results not all axis are given in the same range.

5.1 Joint space safety aware impedance controller

In this section the results of the one degree of freedom safety aware impedance controller will be discussed. During the experiments, the controller as described in Section 2.3 is implemented with the following initial control parameters calculated in Chapter 4:

$$\text{Joint 1}: \; k_0 = 11.829 \; \{\mathrm{N\,m\,s/rad}\} \quad b_0 = 2.9572 \; \{\mathrm{N\,m\,s/rad}\} \tag{5.1}$$

$$\text{Joint 4}: \; k_0 = 5.9898 \; \{\mathrm{N\,m\,s/rad}\} \quad b_0 = 0.7477 \; \{\mathrm{N\,m\,s/rad}\} \tag{5.2}$$

During testing with the KUKA youBot one of the joints broke and therefore the initial position proposed in Chapter 3 can not be achieved . During the experiments the configuration shown in Figure 5.1 is used.

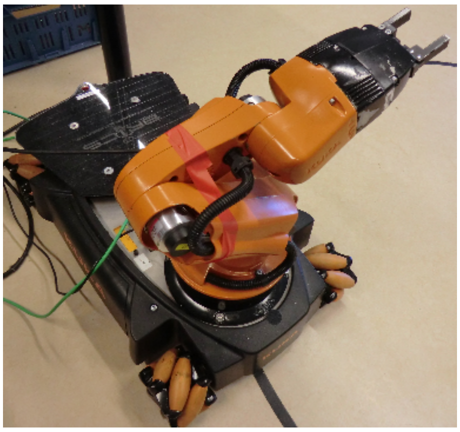

Figure 5.1: Picture of the KUKA youBot in the initial configuration used during the experiments

5.1.1 Free movement without power and energy limitation

First the free motion experiment is performed, without enabling the safety limits of the controller, so only a regular impedance controller is used for controlling the system. As input of the controller, a 3$^{\text{rd}}$ order motion profile with an amplitude of 90° is used in case of controlling Joint 1, a motion profile of 45° is used during the experiments with Joint 4. The motion profiles are chosen such that the maximum output velocities will not exceed the values chosen during the controller design in Chapter 4.

Figure 5.2 shows the results of the free motion experiment. This figure clarifies that the desired performance is not met. The motion error exceeds the desired maximum error. It is expected that the high friction within the joint is the main reason that the desired performance is not obtained, because the friction will dissipate additional power from the controller. This extra loss is seen in the measurement of the energy storage tank which reduces every time the manipulator is moved.

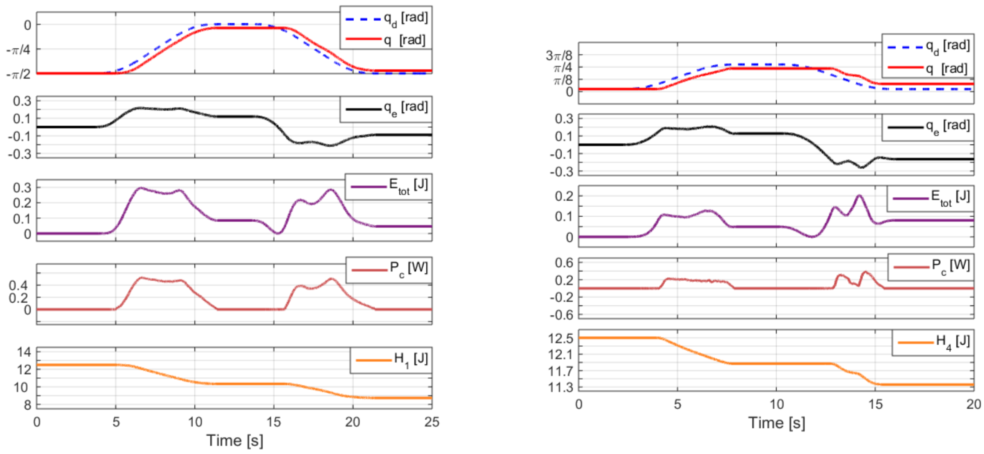

(a) Joint 1 **(b)** Joint 4

Figure 5.2: Experimental results during free motion using a regular impedance controller controller. Desired setpoints q_d, Measured setpoints q, Position error q_e, Total energy of impedance controlled system E_{tot}, Power flow from the controller to the plant P_c, Energy in storage tank H_1.

For that reason a plant compensation controller as explained in Section 4.2 will be used to compensate for the presence of friction. Figure 5.3 shows the results obtained using the additional controller. Within this figure is seen that in case of the first joint the motion error is reduced to the desired maximum error. However for the fourth joint the error during motion is only reduced for a small part which means that the plant compensator doesn't compensate for all the friction. For both cases the steady state error is strongly reduced. Furthermore the maxima of the total energy and power flow are reduced in comparison with the measurements in Figure 5.2. This is expected because the plant compensation controller will introduce additional power to the controlled system and therefore the impedance controller itself will use less power. The influence of adding the plant compensation controller is also seen in the measurement of the state in the energy storage tank which is increasing during the experiment of Joint 1. In the results of Joint 4 is seen that the total energy consumption during motion is reduced by using the plant compensation controller.

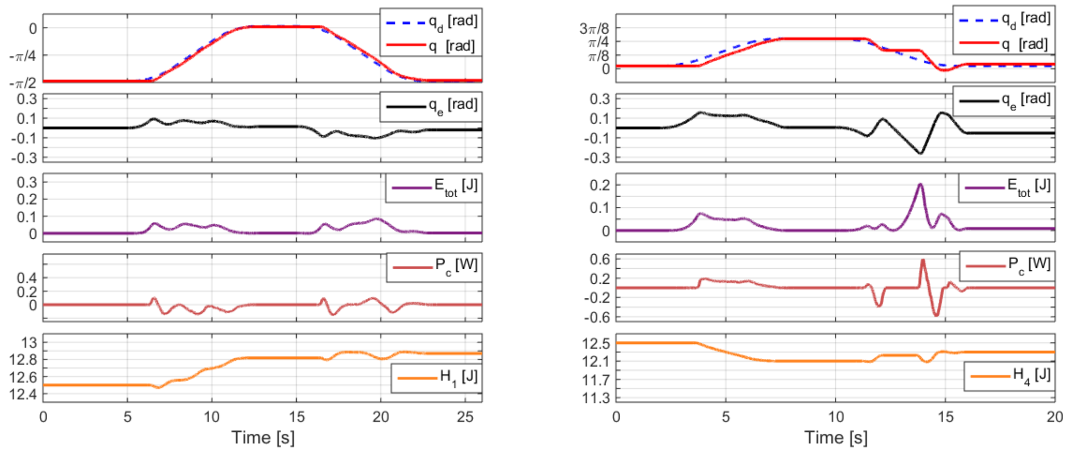

(a) Joint 1

(b) Joint 4

Figure 5.3: Experimental results with free motion trajectory using the regular impedance controller and the plant compensation controller. Desired setpoints q_d, Measured setpoints q, Position error q_e, Total energy of impedance controlled system E_{tot}, Power flow from the controller to the plant P_c, Energy in storage tank H_1,H_4.

5.1.2 Free movement with energy and power limitation

To analyse the performance of the controller using the safety limits explained in Section 2.3 the experiments are performed under the same conditions as in Section 5.1.1. First the results obtained using the safety Aware controller without the plant compensation controller are shown. After that the results with the plant compensation are presented.

Figure 5.4 shows the measurements by using the energy limitation of the safety aware impedance controller. The energy limits are chosen such that it will be reached during motion and the behaviour of the controller can be analysed in that case. From the shown figure can be seen that when the maximum energy is reached, the stiffness k_c and damping b_c are lowered. Also the controller is keeping the required maximum energy. However, the performance of the total system is reduced because the controller is not able to achieve the current setpoints.

The measurements with power limitation are shown in Figure 5.5. In the corresponding figure is seen that the controller is able to maximize the power output by increasing the damping parameter b_c. The motion error is increased in comparison with Figure 5.2 but the steady state errors remains the same.

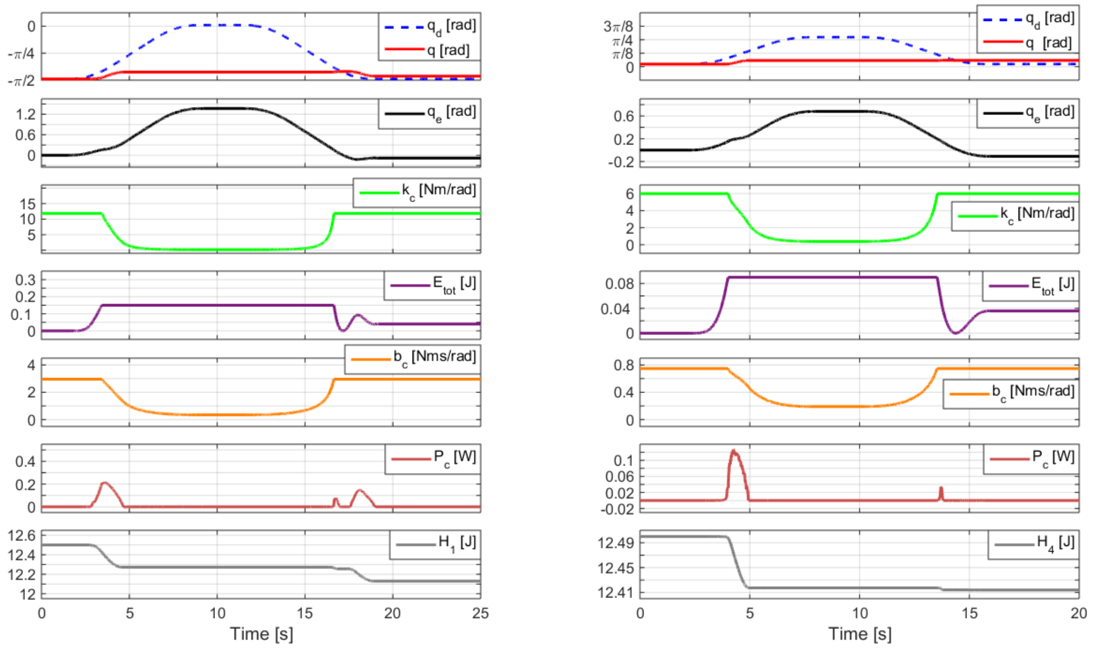

(a) Joint 1 with $E_{max} = 0.15$J **(b)** Joint 4 with $E_{max} = 0.09$J

Figure 5.4: Experimental results with free motion trajectory and energy limitation using the proposed safety aware controller. Desired setpoints q_d, Measured setpoints q, Position error q_e, Control stiffness parameter k_c, Total energy of impedance controller E_{tot}, Control damping parameter b_c, Power flow from the controller to the plant P_c, Energy in storage tank H_1, H_4.

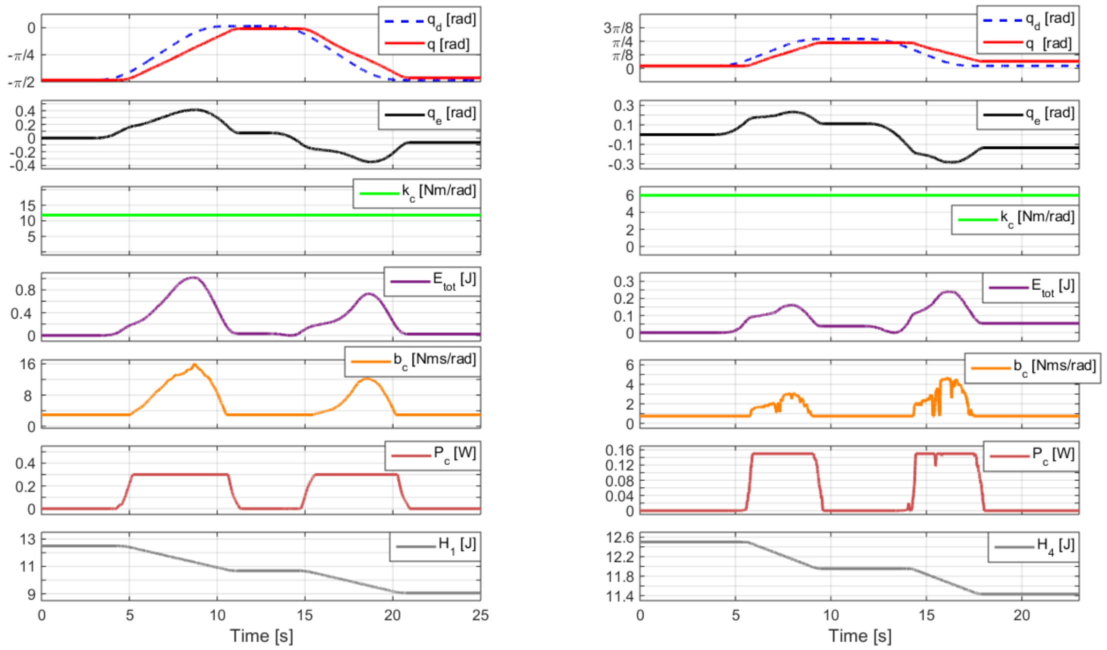

(a) Joint 1 with $P_{max} = 0.3$W **(b)** Joint 4 with $P_{max} = 0.15$W

Figure 5.5: Experimental results with free motion trajectory and power limitation using the proposed safety aware controller. Desired setpoints q_d, Measured setpoints q, Position error q_e, Control stiffness parameter k_c, Total energy of impedance controller E_{tot}, Control damping parameter b_c, Power flow from the controller to the plant P_c, Energy in storage tank H_1, H_4.

Next the results using the safety aware impedance controller with the plant compensation controller are presented. Figure 5.6 shows the achieved results using an energy limitation. By adding the plant compensation controller the controlled system is able to achieve the setpoints in the first part of the motion profile. For the second part the energy is kept at a limit and the request setpoints are not met in this case. In the measurement of the power flow is seen that at certain times it is negative. It is expected that this power flow during deceleration is negative, when it is negative during acceleration the motion is caused by the plant compensation controller. This results in an increase of the energy in the energy storage tank, as is shown in the last measurement of Figure 5.6.

Figure 5.7 shows the obtained results by limiting the power flow from controller to plant. Because the power flow is maximized for small periods of time the influence of this on the controller system is negligible. However, it can be seen that during these moments the damping parameter b_c is increased to keep a maximum positive power flow.

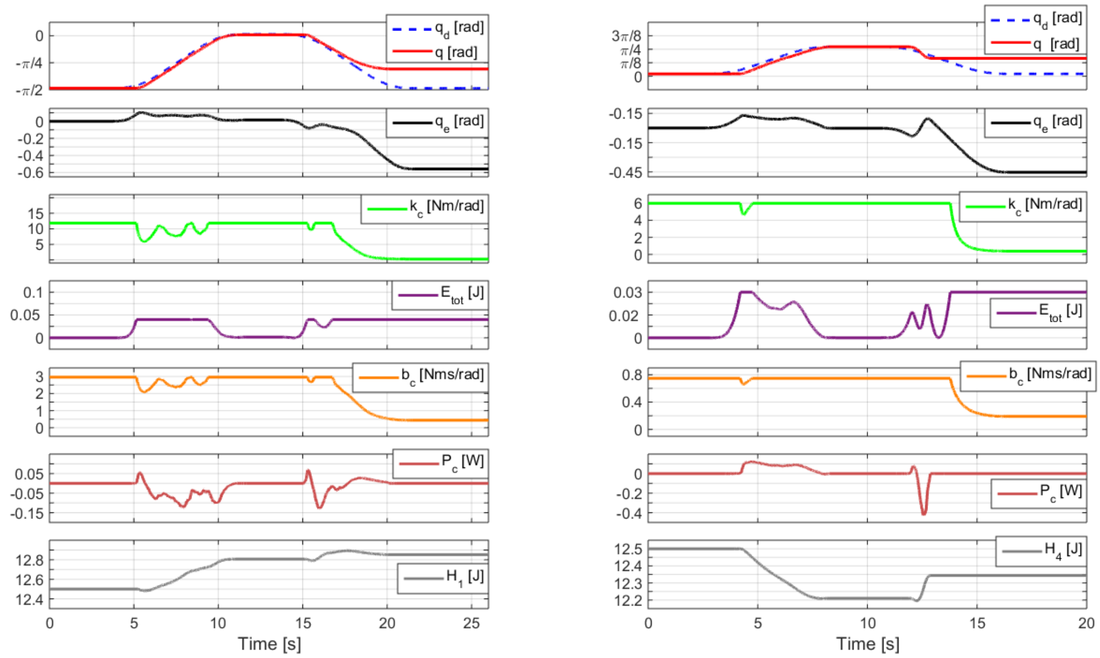

(a) Joint 1 with $E_{max} = 0.04$J

(b) Joint 4 with $E_{max} = 0.03$J

Figure 5.6: Experimental results with free motion trajectory and energy limitation using the proposed safety aware controller and plant compensation controller. Desired setpoints q_d, Measured setpoints q, Position error q_e, Control stiffness parameter k_c, Total energy of impedance controller E_{tot}, Control damping parameter b_c, Power flow from the controller to the plant P_c, Energy in storage tank H_1,H_4.

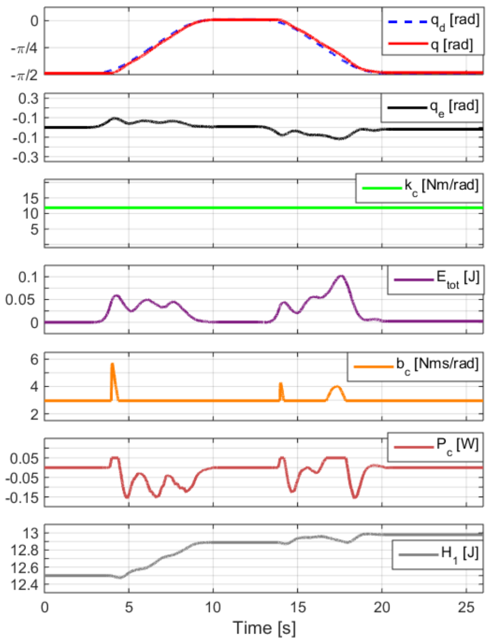

(a) Joint 1 with $P_{max} = 0.05$W

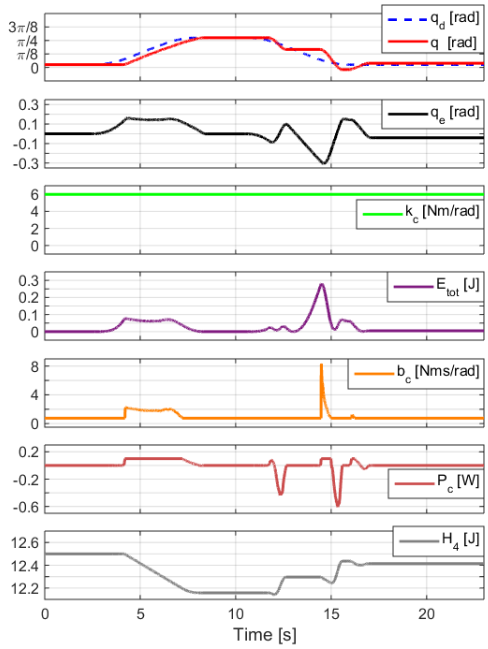

(b) Joint 4 with $P_{max} = 0.01$W

Figure 5.7: Experimental results with free motion trajectory and power limitation using the proposed safety aware controller and plant compensation controller. Desired setpoints q_d, Measured setpoints q, Position error q_e, Control stiffness parameter k_c, Total energy of impedance controller E_{tot}, Control damping parameter b_c, Power flow from the controller to the plant P_c, Energy in storage tank H_1,H_4.

5.2 Cartesian space safety aware impedance controller

Within this section the results using the cartesian space controller will be discussed. It is chosen to use the same control parameters as in case of the joint space controller explained in Section 5.1. Because the configuration of the youBot arm will be the same during motion, the inertia of the manipulator will not change. Therefore the same control parameters can be used. Using the same motion profiles for each joint as used in the previous experiment the expected maximum error will become 0.0125 m for Joint 1 and 0.0068 m for Joint 4.

5.2.1 Free movement without power and energy limitation

Figure 5.8 shows the measurements corresponding to the free motion experiment without the safety limits enabled. It is seen that the maximum expected error of is exceeded and energy is lost during motion. For the same reason as during the joint space experiments a plant compensation controller is used to reduce the influence of friction during movement of the manipulator. The results of this addition are shown in Figure 5.9. Using this figure is can be seen that the error during motion is reduced but is not within the boundaries of the absolute motion error e_{max}. It is also seen that energy in the energy storage tank is added during the experiment of the first joint due to the plant compensation controller. For Joint 4 the total used energy is reduced. Comparing Figure 5.2 and Figure 5.8 there is seen small differences in the amplitudes of the estimated power and energy measurements. These differences are seen because the end effector position in cartesian space is estimated by forward kinematics using the actual joint angle positions. So the travelled distance can differ slightly due small errors in the kinematics.

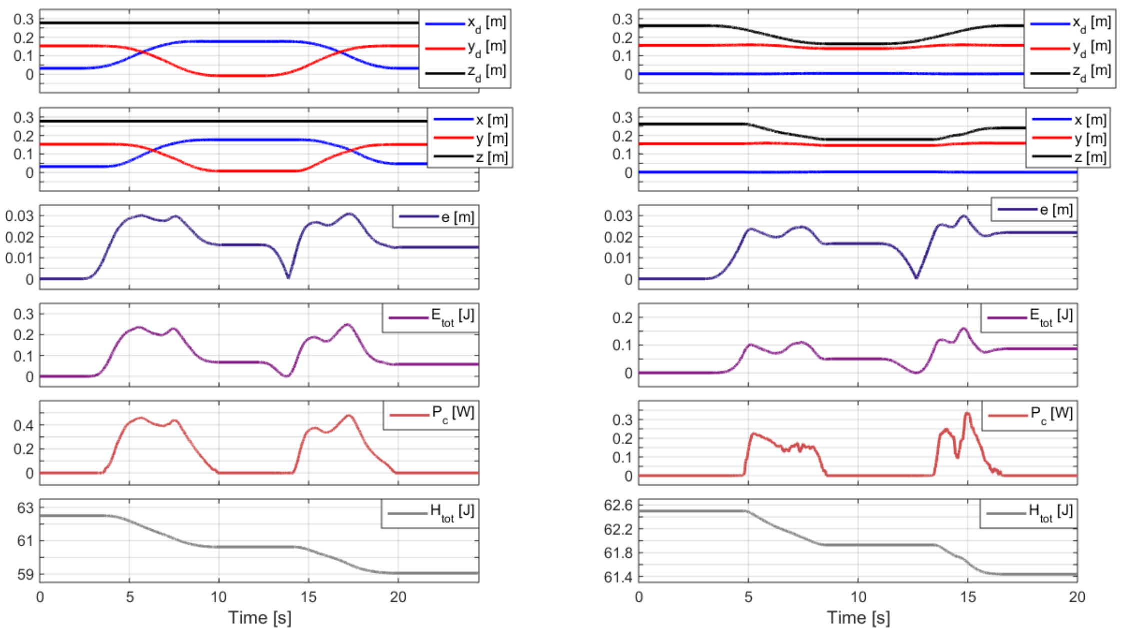

(a) Joint 1 **(b)** Joint 4

Figure 5.8: Experimental results during free motion using a cartesian impedance controller controller. Desired setpoints x_d, y_d, z_d, Measured setpoints x, y, z, Position error e, Total energy of impedance controlled system E_{tot}, Power flow from the controller to the plant P_c, Energy in storage tank H_{tot}.

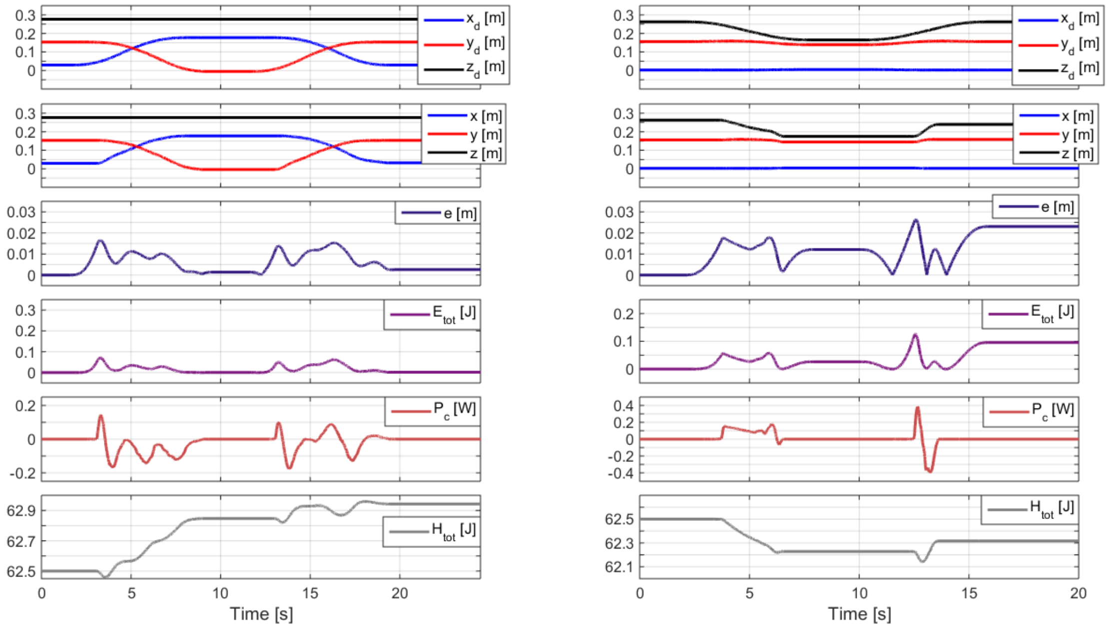

(a) Joint 1

(b) Joint 4

Figure 5.9: Experimental results during free motion using a cartesian impedance controller and a plant compensation controller. Desired setpoints x_d, y_d, z_d, Measured setpoints x, y, z, Position error e, Total energy of impedance controlled system E_{tot}, Power flow from the controller to the plant P_c, Energy in storage tank H_{tot}.

5.2.2 Free movement with power and energy limitation

During the one degree of freedom in Section 5.1.2 is already seen what kind of influence the plant compensation controller has on the total controller. Therefore only results of the safety aware impedance controller with the safety limits enabled will be shown.

Figure 5.10 shows the experiment with the energy limit enabled. By reducing the stiffness scaling parameter λ the controller is able to keep the maximum given energy. In the first part of the motion the energy limitation is only reached for a small amount of time. In the second part of the motion profile the controller is keeping the maximum energy, but resulting in a system which is not able to reach the end position. Because the plant compensation controller uses the current velocity the influence reduces when the velocity of the arm is reducing. And with lowering the stiffness of the controller the output torque is also lowered, which results in a system that will finally stop moving.

In case of the power limitation the measurements in Figure 5.11 are obtained. By increasing the damper scaling parameter β the controller will keep the maximum output power flow to the manipulator. During this control action the system is still able to reach the end point position within the given boundaries.

Furthermore, it is seen that during both experiments the energy in the storage tank is increasing, which means that the plant compensation controller has a significant influence on the behaviour of the total system.

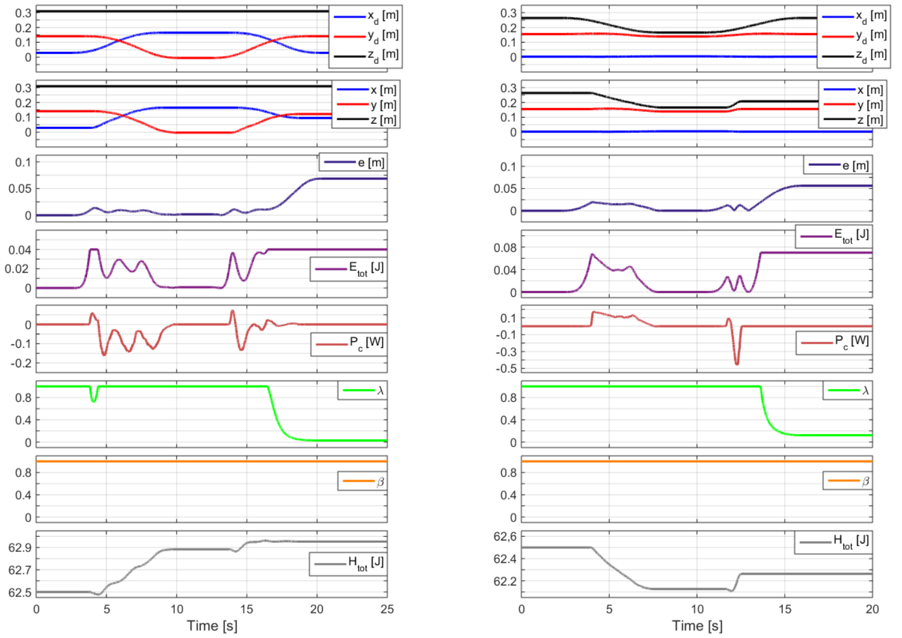

(a) Joint 1 with $E_{max} = 0.04$J

(b) Joint 4 with $E_{max} = 0.07$J

Figure 5.10: Experimental results during free motion and energy limitation using a cartesian impedance controller and plant compensation controller. Desired setpoints x_d, y_d, z_d, Measured setpoints x, y, z, Position error e, Total energy of impedance controlled system E_{tot}, Power flow from the controller to the plant P_c, Stiffness scaling parameter λ, damper scaling parameters β, Energy in storage tank H_{tot}.

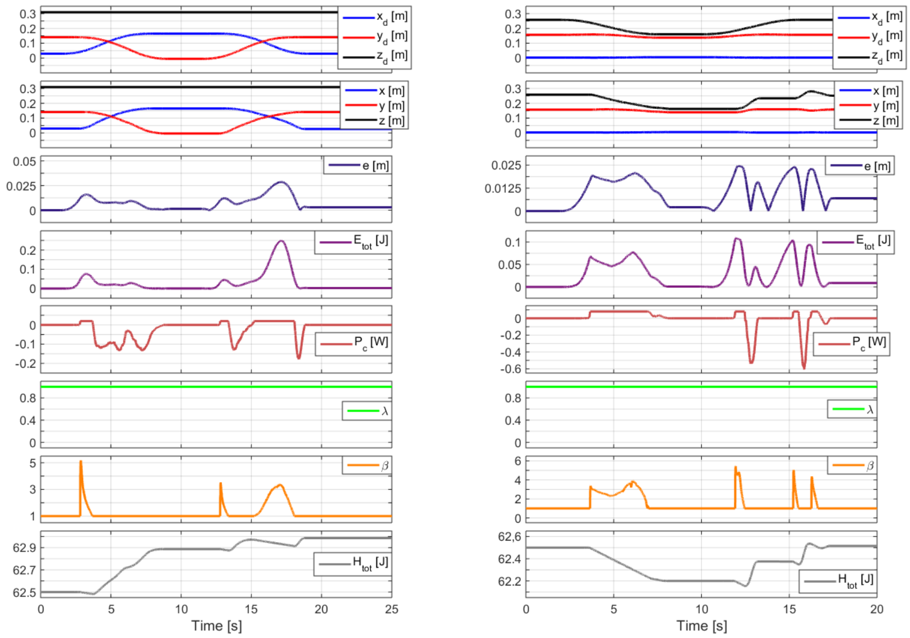

(a) Joint 1 with $E_{max} = 0.02$J

(b) Joint 4 with $E_{max} = 0.08$J

Figure 5.11: Experimental results during free motion and power limitation using a cartesian impedance controller and plant compensation controller. Desired setpoints x_d, y_d, z_d, Measured setpoints x, y, z, Position error e, Total energy of impedance controlled system E_{tot}, Power flow from the controller to the plant P_c, Stiffness scaling parameter λ, damper scaling parameters β, Energy in storage tank H_{tot}.

5.2.3 Collision Path and Human Interaction

In this section is shown the controller while a collision occurs and during interaction with a human. These results are shown in Figure 5.12a and Figure 5.12b respectively. Both experiments are obtained using Joint 1 of the KUKA youBot. For both cases is used an energy limit of $E_{max} = 0.15$J and a power limitation of $P_{max} = 0.25$W. For the collision experiment the motion profile of the previous experiment is used but now with an obstacle in its path. The collision occurs after 8 seconds and at this moment the stiffness scaling parameter is lowered which result in a more compliant system. During this collision the system remains stable and there is no power flow from controller to the manipulator. Furthermore the measurement data are comparable with the obtained results in Section 5.2.2.

During the interaction experiment the manipulator's position changed by a human user. The robotic arm is moved in a positive and a negative direction. As can be seen in Figure 5.12b the stiffness scaling parameter is also reduced as expected. Also the energy in the storage tank is increased due to the movement of the human user.

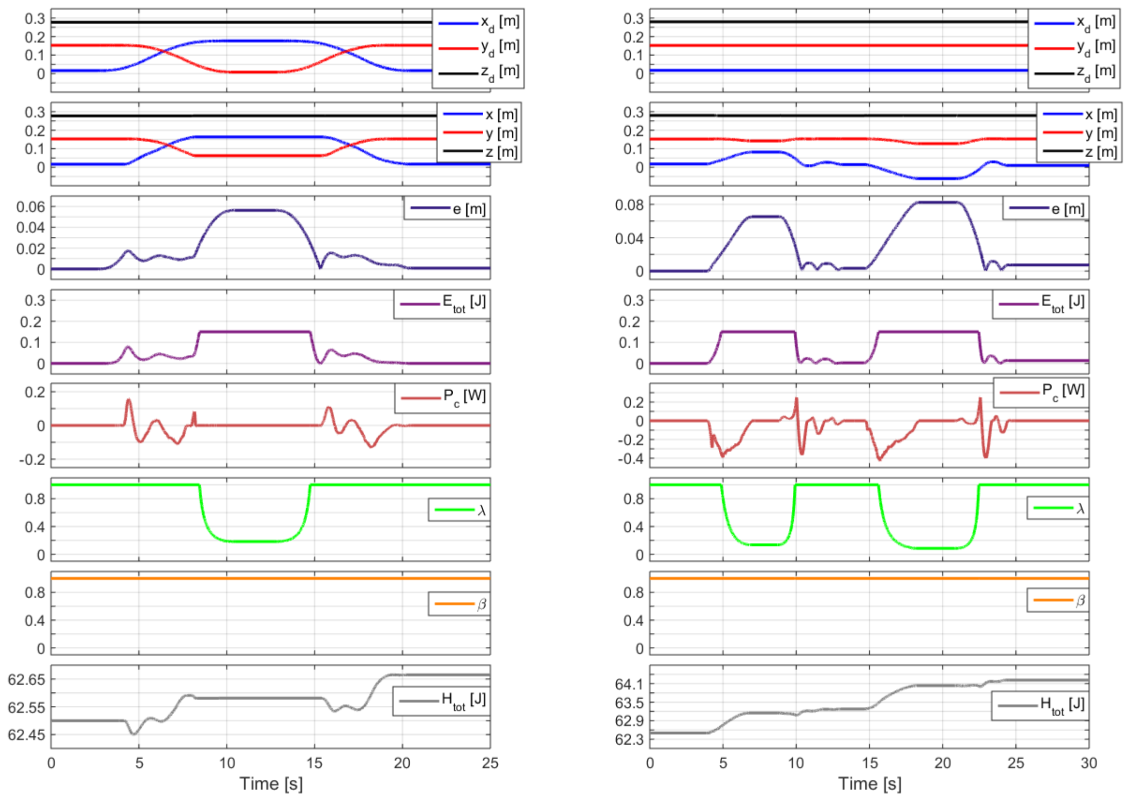

(a) Collision **(b)** Interaction

Figure 5.12: Experimental results of Joint 1 with the cartesian controller during a collision and interaction . Desired setpoints x_d, y_d, z_d, Measured setpoints x, y, z, Position error e, Total energy of impedance controlled system E_{tot}, Power flow from the controller to the plant P_c, Stiffness scaling parameter λ, damper scaling parameters β, Energy in storage tank H_{tot}.

6 Discussion

Within this chapter the results obtained in Chapter 5 will be discussed. The discussion will combine the results obtained by the safety aware impedance controller in joint space and cartesian space.

6.1 Free movement without energy and power limitation joint

During the measurements of the controller without the energy limits enabled it was seen that the performance of the system was highly influenced by the friction in the motor joint. Therefore, a plant compensation controller was implemented to compensate for the loss of energy due to friction. With this additional controller, the system was able operate within the boundaries of the desired performance criteria. However during the control of joint 4 it was seen that the reduction was not the same as seen during the measurements with joint 1. The plant compensation controller only affected the steady state error in that case. In the second part of the motion profile it is seen that the movement is not smooth, it is expected that this is due to a high stiction force at that location because it occurs at the same location every time. A drawback of using the plant compensation controller is the loss of passivity, which was one of the design criteria of the safety aware impedance controller. This loss of passivity is seen in the measurement of the state of the energy storage tank. The energy of this tank is increased during the motion which means that additional energy is added to the controlled system. This is seen in the measurement of the power flow from controller to plant where at certain times the power is negative during acceleration of the plant which means that this power is inserted in the controller. But when the plant compensation controller will not be used the system is only able to move a certain amount of times before the total energy tank is depleted.

Comparing the obtained results with the impedance controller in joint space and cartesian space, it is seen that they have the same performance considering the energy and power measurement. This is expected because only the reference point is changed which may not effect the dynamical behaviour of the system. Comparing Figure 5.2 and Figure 5.8 it is seen that there is only a small difference in amplitude of both signals but the overall behaviour is the same. In case of the measurements of joint 4 it is observed that the steady state error is not reduced close to zero with the addition of the plant compensation controller during the cartesian space measurements. Because during this control more joint are taken into account an error in the other joints will also effect these measurements.

6.2 Free movement with energy and power limitation joint

During the experiments with the safety limits enabled it has been shown that the controller behaves as expected. The values of the control parameters are changed to keep the desired limits, doing so the controller does not loss its stability. Only the performance with respect to the error is reduced, but this is expected because limiting the power output or expected kinetic energy will affect its behaviour. It should be noted that the used limits are chosen for testing purpose only. They do not represent values which will be used during a real practical application but are chosen such that influence of changing the control parameters could be tested. The change of the one degree of freedom controller by changing the damping parameter b_c together with the stiffness parameter k_c during energy limitation did not affect the total stability of the system, but during the experiment it is seen that it has improved the performance. Using this implementation the controlled system was now able to reach the desired setpoints while limiting the energy, which was not the case with the initial implementation.

Figure 5.4 shows the measurements of the free motion profile while using an energy limitation without compensating for friction. In the measurement of the position it is seen that the controller is not able to reach the desired setpoints when the energy limit is reached. This behaviour is not seen in Figure 5.6 where a plant compensation controller is used. The difference in both cases can be explained by Equation (4.2). During the derivation of this equation the occurrence of friction is not taken into account and with that the loss of energy. Due to this the system without using friction compensation will reach the maximum energy sooner and therefore is not able to met the desired performance. So from this can be concluded that the proposed controller can only be used in two different cases: in a system without friction or in a system where the friction is partially compensated. The friction has to be partially compensated to be sure that there is no overcompensation of the friction which leads too a larger controller torque than desired.

Although while using the plant compensation the system looses the passivity it is still able to use the safety limits because the actual joint velocities are used. So in the measurements with the use of the plant compensation controller the controlled system is still able to keep the maximum energy and power level but with a lower error during motion. As is shown in Figure 5.6 and Figure 5.10, the system is not able to reach the desired end position within the desired error boundaries in the second part of the motion profile. To keep the maximum energy the stiffness of the controller is lower to obtain a more compliant system. However the system became to compliant in this region, resulting is a system which is not able to reach the desired end position.

6.2.1 Collision Path and Human Interaction

During the experiments with collision it is seen that the total system remains stable during the collision. The manipulator is still able to follow the commanded motion profile when it is moving away from the obstacle and reach the end position within the desired error limits. During collision the stiffness scaling parameter is decreased such that a more compliant system is obtained.

Interaction with the manipulator is done by moving the manipulator by hand. The youBot arm is moved in the positive and negative direction and during these actions the stiffness scaling parameter is lowered to maintain the desired energy limit and to get a compliant system. Figure 5.12b shows that when the manipulator is released again the system is controlled to the initial position. In the measurement of the energy storage tank it is seen that it is increasing during displacement of the robotic arm. This is expected because the human user adds extra energy while moving this arm. However this additional energy should be removed again when the manipulator is controlled to its initial position, but this is not the case because the plant compensation controller is limiting this loss. It is even seen in this case that it adds additional energy to the storage, because the friction is lower then is expected in the plant compensation controller. This is not desired and therefore it will be advised to partially compensate for friction such that overcompensation is avoided.

7 Conclusion & Recommendations

7.1 Conclusion

For the one degree of freedom safety aware impedance controller in joint and cartesian space it is possible to control a manipulator to desired setpoints. Using the proposed safety limits the power output and kinetic energy of the robotic arm can be maximized resulting in a system which is considered safe under the given conditions. The implementation change of the one degree of freedom implementation to keep a constant damping ratio did not affect the stability of the system but while using this implementation the performance was improved.

To test the controller in multiple degrees of freedom, the cartesian space implementation is used. From these test can be concluded that by changing the scaling parameters the safety limits are kept while keeping the total system stable.

Although all the tests are performed by actuation of a single joint it can be concluded that the controller will also work while actuating multiple joints because it is shown that the controller behaves as expected during controller of different joints.

Using a plant compensation controller the available friction within the joints of the manipulator is compensated. This resulted in a system with better performance, however it affects the passivity of the controlled system which was one of the design criteria. Therefore the compensation of friction should be done partially such that no overcompensation of friction occurs.

During interaction and collision the controller maintains stable while the scaling parameters are changed to keep the desired safety limits.

7.2 Recommendations

Because the passivity of the controlled system is an important part in the design of the proposed safety aware controller it is recommended to change the controller such that with the addition of a friction compensator the controlled system is still passive. In future research the proposed safety aware controller should keep the capability of limiting the power flow and energy output but also the performance by compensating for friction. This could be achieved by partially compensation of the friction, resulting in a system which should have a desirable performance without exceeding the initial energy in the storage tank.

Now the controller is tested on a more complex system the next task is to implement the safety aware controller of on the Phillips robotic arm where is was originally designed for. Using this implementation the controller can be tested while performing tasks which will be commonly used in a domestic area. Furthermore the controller can be tested with the different parts of the BOBBIE project.

It is also recommended to have further research into the safety limits of the controller. It should be identified which kind of values are needed to have a save controlled system without inflicting damage to the surroundings.

Bibliography

Bobbie Robotics (2014), About Bobbie Robotics.
http://www.bobbierobotics.nl/home

de Boer, H. (2012), *Modeling and control of the Philips Robotic Arm*, Master's thesis, University of Twente.

Brodskiy, Y., R. J. W. Wilterdink, S. Stramigioli and J. F. Broenink (2013), Collection of methods for achieving robust autonomy, Deliverable FP7 BRICS Project (231940) D6.2, University of Twente.

Controllab products (2015), 20-sim.
http://www.20sim.com/

Dresscher, D. (2011), *Robust Autonomy for the youBot*, Msc report 003ce2011, University of Twente.
http://essay.utwente.nl/60143/

Ferretti, G., G. Magnani and P. Rocco (2004), Impedance control for elastic joints industrial manipulators, **vol. 20**, no.3, pp. 488–498.

Frijnts, S. D. (2014), Upgrading the Safety Layer and Demo of the youBot Robot, Pre-msc report 007ram2014, University of Twente.

Haddadin, S., A. Albu-Schaffer and G. Hirzinger (2008), The role of the robot mass and velocity in physical human-robot interaction - Part I: Non-constrained blunt impacts, in *Robotics and Automation, 2008. ICRA 2008. IEEE International Conference on*, pp. 1331–1338, ISSN 1050-4729, doi:10.1109/ROBOT.2008.4543388.

Hogan, N. (1985), Impedance control: An approach to manipulation: Part II - Implementation, **vol. 107**, no.1, pp. 8–16.

Ikuta, K., H. Ishii and M. Nokata (2003), Safety Evaluation Method of Design and Control for Human-Care Robots, **vol. 22**, no.5, pp. 281–297, doi:10.1177/0278364903022005001.
http://ijr.sagepub.com/content/22/5/281.abstract

KUKA Laboratories (2014), KUKA Youbot.
http://www.kuka-labs.com/en/service_robotics/research_education/youbot/

Orocos Project (2015), Smarter control in robotics & automation.
http://www.orocos.org

Stramigioli, S. and H. Bruyninckx (2001), Geometry and screw theory for robotics, *Tutorial during ICRA*, **vol. 2001**.

Tadele, T., T. de Vries and S. Stramigioli (2013), PID motion control tuning rules in a damping injection framework, in *American Control Conference (ACC), 2013*, pp. 4957–4962, ISSN 0743-1619, doi:10.1109/ACC.2013.6580607.

Tadele, T. S., T. J. A. de Vries and S. Stramigioli (2014a), Performance Based Analysis and Impedance Control Design for Human-friendly Manipulators.

Tadele, T. S., T. J. A. de Vries and S. Stramigioli (2014b), Safety aware impedance controller design for human-friendly manipulators.